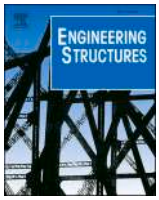
Engineering Structures 322 (2025) 119189



Contents lists available at ScienceDirect

Engineering Structures

journal homepage: www.elsevier.com/locate/engstruct





Utilization of strain-hardening cementitious composites to restore the efficiency of square RC columns after fire exposure

Abd El-Hakim A. Khalil, Tarek F. Elshafiey, Ahmed T. Baraghith *, Reda N. Behiry, Hanan Ali

Structural Engineering Dept., Faculty of Engineering, Tanta University, Tanta, Egypt

ARTICLE INFO

Keywords:
Fire
Columns
Strain-Hardening Cementitious Composites (SHCC)
Repair
Axial capacity
Stiffness
Finite element analysis

ABSTRACT

Reinforced concrete (RC) is well-recognized as a fire-resistant construction material. Even though, severe fire exposure can change the physical and chemical properties of concrete and steel, causing some level of damage to RC structures. As a practical solution to these problems, strain-hardening cementitious composites (SHCC) have been used in this study to repair the post-fire square RC columns. So far, a total of 13 specimens have been prepared and tested under axial compression. The full experimental program involved: (1) one non-damaged/non-repaired reference column; (2) five post-fire/non-repaired columns; and (3) seven post-fire/SHCC-repaired columns. The test variables included the fire exposure duration (1, 2, or 3 hrs.), temperature level (400 °C, 600 °C, or 800 °C), and thickness of the SHCC jacket (20 mm, 30 mm, or 40 mm). The results indicated that using the SHCC jacket was effective in terms of the restorability of the load-carrying capacity, secant stiffness, and energy absorption of all tested post-fire RC columns even more than the reference specimen at ambient temperature (20 °C). The enhancement percentages in the load-carrying capacity varied between 17 % and 151 %, depending on the test parameters. In addition, SHCC-repaired columns exhibited on average 16 % higher axial stiffness and a larger energy absorption capacity when compared to the reference non-damaged column. A three-dimensional (3D) non-linear finite element model (FEM) was carried out using ABAQUS software and validated against the experimental results in order to further evaluate the potential of the SHCC jacket to restore the efficiency of fire-damaged columns. Finally, test results were utilized to verify an engineer-friendly formula that was derived to predict the load-carrying capacity of post-fire/repaired RC columns to promote their evaluation in engineering practices.

1. Introduction

To this day, concrete continues to be one of the most commonly used structural materials worldwide. This is primarily due to their locally available ingredients, durability properties, and cost-effectiveness. In addition, it is also a versatile material for architectural and structural applications, which, in turn, positively impacts the economic progress of countries. In skeleton buildings, RC columns are the most critical elements; if one of them fails, the structure may partially or completely collapse. Structural system changes, construction errors, increasing traffic volumes, damage caused by unexpected overloading, blasts, earthquakes, and fire exposure can all lead to the deterioration of RC columns [1,2].

The National Fire Protection Association (NFPA) estimates that in 2020 there were 2730 civilian deaths and 13,000 injuries as a result of the 490,500 residential building fires that occurred in the United States [3]. These numbers highlight that fire seriously threatens people's lives and thus drew the researchers' attention to the urgent need for understanding the behavior of RC structures during and after fire. Many of the current studies on fire are based on the test procedures and fire curves described in ISO 834 [4] and ASTM E119 [5] specifications. These standard fire tests have been the dominant method of indicating the behavior of RC structural elements in fire [6–11].

In general, upon exposure to high temperatures in an aggressive fire, concrete is non-flammable and has a low thermal conductivity. This protects the steel bars to some extent and gives RC structures higher fire resistance than steel or wood ones. However, the mechanical properties of concrete (e.g., compressive strength and elastic modulus) degrade, which reduces the elements' capacity and the structure's stability. One possible explanation is that an increase in temperature causes thermal expansion of concrete, plastic deformation of steel, and hence incompatibility between steel and surrounding concrete [12–17].

* Correspondence to: Structural Engineering Dept., Faculty of Engineering, Tanta University, Tanta 31511, Egypt.
E-mail addresses: ahmed.baraghit@f-eng.tanta.edu.eg, ahmed_baraghit@yahoo.com (A.T. Baraghith).

https://doi.org/10.1016/j.engstruct.2024.119189
Received 30 January 2024; Received in revised form 6 October 2024; Accepted 19 October 2024
Available online 29 October 2024
0141-0296/© 2024 Elsevier Ltd. All rights are reserved, including those for text and data mining, AI training, and similar technologies.

Researchers have conducted several studies to understand the behavior of post-heated RC columns. The studies [18–30] listed in Table 1 demonstrate that when RC columns are exposed to elevated temperatures, there are two main consequences: capacity reduction and stiffness degradation, which result in a negative impact on structures. Nevertheless, real experiences reveal that most RC structures can be effectively repaired following a fire, and it is quite unusual that a concrete building collapses.

Since repairing concrete structures is more cost-effective than destruction and total or partial reconstruction, it has become widespread in the construction industry. To restore the strength and stiffness of concrete structures following a fire, various methods were developed [1,31]. One popular method is surrounding the original column with a reinforced concrete jacket, which increases the cross-sectional area. Consequently, given its inability to improve the ductility during earthquakes [32]. In contrast to concrete, steel loses over half of its yield stress and elastic modulus at about 400–500 ℃, making steel jackets more susceptible to elevated temperatures than concrete ones [33]. Based on previously published research, the application of fiber-reinforced polymer (FRP) wrapping can effectively improve the strength and ductility of post-fire structures [6,31–39]. However, the lack of stiffness's restorability is a major drawback, which makes the FRP wrapping system impractical to use [39]. Moreover, rectangular columns (the most common in practical projects) confined with FRP exhibit different performance compared to circular ones because the entire section is not effectively confined. The confinement action in rectangular-section columns is concentrated near the corners [32].

Nowadays, Engineered Cementitious Composites (ECC), a new category of fiber-reinforced cementitious composites introduced in 1992 by Li and coworkers [40], shows a good promise as an alternative repair material to overcome the previous deficiencies of the aforementioned materials. Typically, ECC mix is designed by mechanistically tuning the cementitious matrix (e.g., cement, sand, and silica fume (SF), non-metallic fibers of a volume fraction less than 2 %, and superplasticizer (SP)) [41]. ECC, also called strain-hardening cementitious composites (SHCC), reaches an ultimate strain capacity of 3–5 % under uniaxial tensile tests and shows tensile pseudo strain-hardening behavior rather than softening [42]. Furthermore, SHCC has the capability to control the crack width, which improves the durability aspects of the structure. Reinforcing SHCC with discrete fibers achieves its strain-hardening and crack-resistance properties. By dispersing these fibers in a cementitious matrix, the bridging effect can be achieved, preventing the cracks in the matrix from widening. As a result, SHCC exhibits enhanced energy absorption, ductility, and damage tolerance. This illustrates the more and more expanding of SHCC in structural applications for strengthening and repair purposes [43–53].

According to recent research [54–56], SHCC outperforms other materials in terms of fire resistance. Fire tests revealed a notable phenomenon: using SHCC prevented explosive spalling, which relieved the deterioration of the mechanical properties and maintained the overall integrity of the tested specimens. The use of polymeric fibers, like polypropylene (PP) fibers, caused the spalling resistance. These fibers melt at elevated temperatures and provide interlinked paths for the release of internal vapor pressure, which is caused by both water evaporation and the thermal decomposition of concrete [55]. All in all, the above-mentioned features allow for new research opportunities into the possibility of using these materials to restore the efficiency of fire-damaged concrete elements.

Table 1
Main findings of previous studies on the behavior of fire-damaged RC columns.

Study	Main findings
Lie and Woollerton [18]	• The change in the amount of longitudinal reinforcing steel in the columns produces relatively small increases in fire resistance.
Dotreppe et al.[19]	• The increase in concrete cover had a positive effect on fire resistance.
Chan et al.[20]	• The compressive strength of concrete may decrease by up to 50 % when it is exposed to more than 600 °C.
Aldea et al.[21]	• The material characteristics have a higher influence on failure modes under fire conditions than the structural detailing.
Kodur and McGrath [22]	• RC columns with a hooked tie configuration (bent at 135° and with closer tie spacing) achieve improved fire performance.
Chen et al.[23]	• The residual load-carrying capacity and the stiffness decreased as the fire exposure time increased.
Wu et al.[24]	• Increasing the dimension of the columns cross-section was an effective measure for improving the fire resistance of RC columns.
Kodur et al.[25]	• The residual strength of a fire-exposed RC column is affected by the internal temperatures, load level during the fire event, cooling method, and rate.
Hibner[26]	• The 90-minute and 120-minute fire-exposed RC columns could retain 34 % and 29 % of their real nominal capacity, respectively.
Buch and Sharma[27]	• Spalling is more serious and widespread in high-strength concrete columns compared to normal-strength concrete ones.
Sharma et al.[28]	• The strength of concrete decreases with increasing temperature, and 600 °C is the critical temperature for serious deterioration in concrete.
Nair and Salem[29]	• The residual axial capacity was reduced to 50 % and 30 % of its original capacity for 1-hour and 2-hour fire exposure, respectively.
Al-Naqeeb and Al-Thairy[30]	• An increase in fire temperature resulted in a reduction in the load-carrying capacity with an increase in the deformation of the tested columns.

2. Research significance

Plenty of previous literature has primarily focused on the restoration of fire-damaged RC columns using traditional concrete jackets or FRP wrapping. On the other hand, the use of strain-hardening cementitious composites (SHCC) in this regard is very limited, despite their well-known merits. In order to fill this gap, this study uniquely exposes the applicability of replacing the concrete cover only with a thin SHCC jacket to improve the performance of such columns. This novel technique aims to address the drawbacks of previous techniques, including those related to ductility and stiffness response. In addition, preventing excessively high dead loads, thus achieving optimal utilization of the building's architectural space, which is considered a crucial consideration, especially in high-density urban areas where every square meter of space is valuable.

In this context, an experimental program was conducted to show how the studied parameters, specifically the duration of fire exposure, temperature level, and the use of SHCC jackets with varying thicknesses, affect the behavior of the repaired post-fire RC columns. Furthermore, to better assess the SHCC jacket's potential for rehabilitating fire-damaged columns, a three-dimensional (3D) non-linear finite element model (FEM) was carried out using ABAQUS software and validated against experimental data. Finally, a suggested equation that predicted the ultimate load-carrying capacity of the tested columns was derived.

3. Experimental work

3.1. Material properties

According to the supplier-provided data sheet, Table 2 shows the proportions of the used ready-mix concrete, where the binder was Portland cement (Type I). Natural siliceous sand (maximum diameter of 4.0 mm) with a 2.20 fineness modulus and a 1650 kg/m^3 bulk density was utilized as fine aggregate. Crushed limestone type 1 (maximum size of 16 mm) was used as the coarse aggregate due to its local availability, cost-effectiveness, and beneficial impact on concrete workability and durability. Along with the specimens, additional cylinders measuring 150 × 300 mm were cast to determine the concrete's compressive

Table 2
Mix proportions per meter cubic of NSC and SHCC materials (kg/m^3).

Concrete mix	W/B	Cement	Sand	Coarse pink limestone	Water	Silica fume	Super-plasticizer	PP Fiber (12 mm)
NSC	0.50	350	750 ($\varnothing \leq 4.0mm$)	1250	175	—	—	—
SHCC	0.20	1243	149 ($\varnothing \leq 0.5mm$)	—	293	223	14.9	16.2

NSC = Normal Strength Concrete; SHCC = Strain-Hardening Cementitious Composites; W/B = water/ binder ratio; B = cement + silica fume; ∅ = diameter of sand particles.

strength. Uniaxial compressive tests were conducted on the testing day of the columns (6 months after concrete casting), in accordance with ASTM C39/C39M-21 [57], and the average ambient cylinder compressive strength was 20.9 MPa.

As listed in Table 2, a cubic meter of SHCC includes 1243 kg of ordinary Portland cement (52.5 R) and 223 kg of silica fume as a binder. The utilized fine aggregate was continuously graded sand, which had a weight of 149 kg/m^3 and a diameter of less than 0.5 mm. In line with the characteristics of SHCC, intentional removal of coarse aggregates was performed to control crack width. Polypropylene microfibers (PP) with a 0.012 mm diameter and a 12 mm length were used, constituting approximately a volume fraction of about 1.5 %. Referring to the manufacturer's data sheets, the used PP fibers have a tensile strength of 150 MPa, an elastic modulus of 3.0 GPa, and an elongation of 8 %. The ratio of water to binder, or w/b, was approximately 0.20, and to improve matrix flowability, a superplasticizer (14.9 kg/m^3 weight) served as an additive with a high water-reducing ability. The mechanical properties of the used SHCC materials were determined according to the ASTM standards [57,58]. The average cylinder compressive strength and Poisson's ratio were 67.90 MPa and 0.252, respectively (see Fig. 1). In addition, the uniaxial tensile strength of SHCC, resulting from the test of three dog-bone specimens [59,60], was 8.48 MPa (see Fig. 2).

Longitudinal reinforcement in the original column consisted of 12 mm-diameter ribbed steel bars, whereas transverse reinforcement was provided by 8 mm-diameter normal mild bars. To improve the cracking behavior, a slight amount of reinforcement (6 mm or 8 mm-diameter plain smooth bars) was provided inside the SHCC jacket. The mechanical properties of the used reinforcement bars were experimentally measured in accordance with ASTM A615/ A615M-16 [61]. For 6, 8, and 12 mm bar diameters, the tensile yield strengths at ambient temperature were 235, 301, and 436 MPa, respectively, and the ultimate values were 472, 487, and 579 MPa.

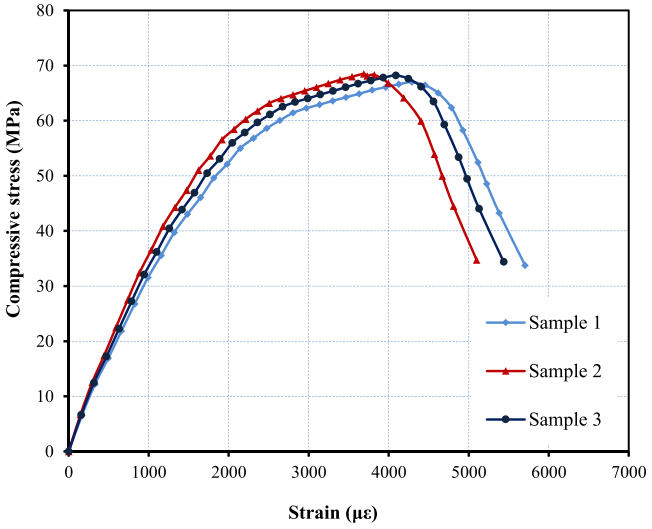


Fig. 1. Compressive stress-strain diagrams of SHCC specimens.

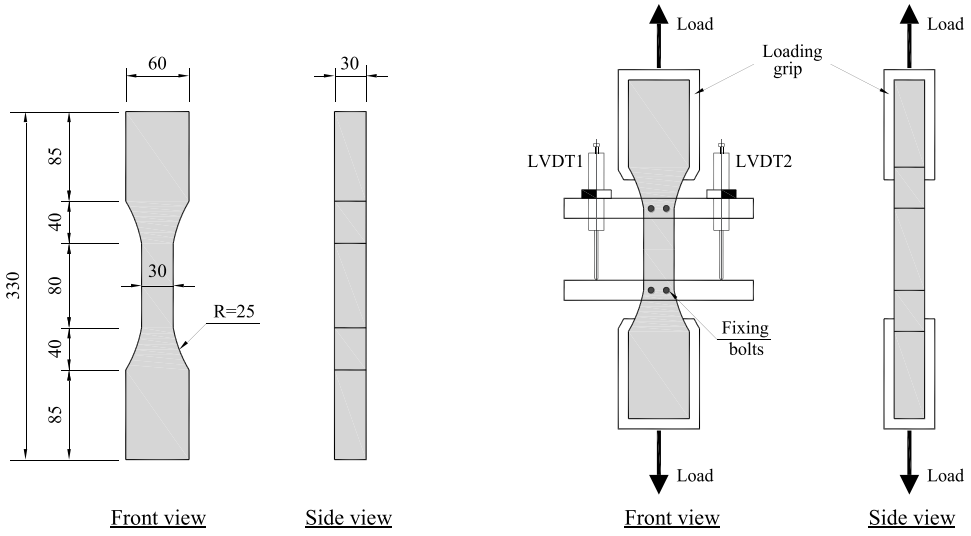
3.2. Description of the tested specimens

Thirteen reinforced concrete square columns (one-third scale) of 200 mm × 200 mm and a height of 1000 mm were cast. The height of the test specimens was limited by the available fire furnace. In compliance with ACI 318–19 [62], four deformed bars with a diameter of 12 mm were embedded inside the original column as longitudinal reinforcement, giving a reinforcement ratio ($\rho_g = A_{SL}/A_g$) of 1.13 %, where A_{SL} is the total area of the longitudinal steel and A_g is the total cross-sectional area of the column. Moreover, 135° hooked transverse ties with smooth bars of 8 mm diameter and spaced 160 mm center-to-center were used in the middle region of the tested columns. The distance between the transverse ties at both columns' ends was lowered to 80 mm in order to prevent any local failure. It is worth mentioning that the clear side and top concrete covers were maintained at 20 mm. Reinforcement details and concrete dimensions are presented in Fig. 3.

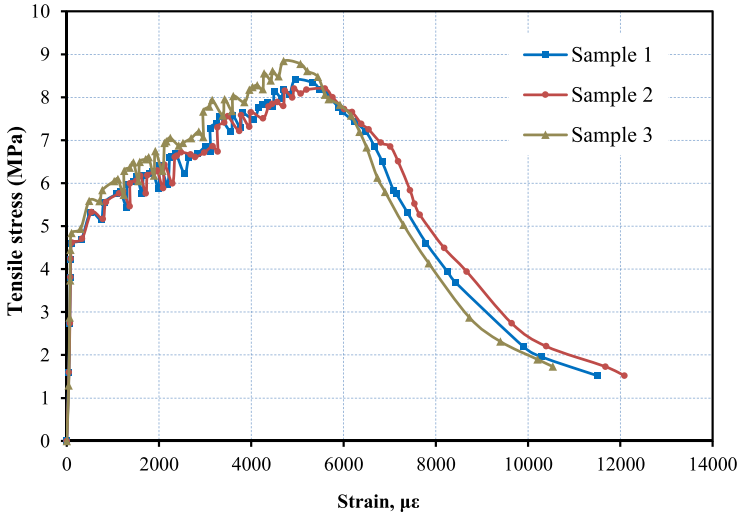
The test matrix was selected to include a wide range of parameters: (i) fire duration (1, 2, or 3 hrs.); (ii) temperature level (ambient, 400, 600, or 800 °C) and (iii) thickness of the SHCC jacket (20, 30, or 40 mm). It is worth mentioning that this temperature range is justified and consistent with that adopted in EN 1992–1-2 [63] as well as previous research [64–67]. Each specimen has a unique identification number ($CX_{A\text{-}B\text{-}C}$), where "CX" denotes the control column (CC) or the repaired column (CR); "A" represents the temperature level; "B" designates the fire duration; and "C" denotes the thickness of the SHCC jacket. For example, specimen "$CR_{600\text{–}2\text{-}20}$" was specifically designed to withstand two hours of 600 °C fire before being repaired with a 20 mm SHCC jacket. As shown in Table 3, the experimental program included: (1) one non-damaged/non-repaired reference column; (2) five post-fire/non-repaired columns; and (3) seven post-fire/SHCC-repaired columns.

3.3. Fire process

The "unstressed residual strength test" procedure was adopted in the current work. The furnace of the National Housing and Building Research Center in Egypt was used, measuring 1.20 × 2.00 × 4.00 m, as depicted in Fig. 4. The fire was provided by four gas burners, with two burners on each side, and the temperature was monitored using thermocouples placed at various locations to ensure uniform heating and consistency and reproducibility of the results. In the beginning, the columns were placed in the furnace manually. In addition, cylinders with dimensions of 150 × 300 mm were placed in the furnace and exposed to the same fire conditions as the columns to determine the mechanical properties of concrete after fire. The fire exposure history used in this study (see Fig. 5) was chosen to simulate real-world scenarios where structures are exposed to prolonged periods of elevated, steady temperatures [6,33,37,68]. Accordingly, the heating rate followed the ISO 834 standard fire curve until reaching the desired furnace temperature, and then the temperature was maintained at a constant level for the required duration. Finally, the furnace turned off automatically, and the specimens were transferred and allowed to cool off



(a) Specimen's dimensions (b) Test setup [59,60]



(c) Obtained stress-strain diagrams

Fig. 2. Uniaxial tensile testing of the dog-bone shaped SHCC specimens.

naturally at ambient temperature for three days.

As listed in Table 4, the compressive strength (measured on the testing day of the columns) was 14.57, 10.77, and 7.23 MPa after exposure to 600 ºC for 1, 2, and 3 hrs., and 14.40, 5.70 MPa when exposed to 400 °C and 800 °C for 2 hrs. As for the steel reinforcement, additional columns were placed in the furnace at each desired temperature. After completing the fire process and cooling, the steel bars were extracted from these columns, and a tensile test was conducted. The tensile yield strengths of 12 mm-steel were 393, 310, and 275 MPa after exposure to 600 ºC for 1, 2, and 3 hrs., and 385, 270 MPa when exposed to 400 °C and 800 °C for 2 hrs.

Throughout concrete casting, two thermocouples of the K-type were embedded in the mid-height of each specimen in order to trace the temperature. One was positioned 20 mm away from the concrete surface (TC-1), and the other was located in the column's center (TC-2). A high-precision data acquisition system was used to collect the temperature data at regular intervals during the heating period. An examination of the temperature homogeneity between specimens was performed through: (1) the data were analyzed to assess the uniform distribution of temperature between the specimens; (2) the degree of temperature uniformity was evaluated by comparing the temperature readings taken at various locations at regular intervals (every 5 min); and (3) the specimens exhibited a high level of homogeneity in terms of temperature, as shown by the thermocouples. The measured temperature difference between the specimens and their counterparts throughout the fire process was less than 5 %. Fig. 6 depicts the average temperature-time curves measured for the specimens during the fire process. Each graph includes the ISO 834 standard fire curve, the average furnace temperatures, and the temperatures measured by two thermocouples (TC-1 and TC-2). Overall, all specimens show a consistent temperature evolution trend. The temperatures within the concrete grew along with the furnace temperatures. However, the rate of increase was inversely proportional to the concrete depth.

3.4. Assessment of fire-damaged columns

Following the fire process, each column was visually inspected to ascertain the extent of fire damage. Fig. 7 depicts the state of the specimens after fire exposure. As expected, discoloration was noticed in all columns after fire exposure. It may be attributed to the physical and chemical transformations in the cement paste and aggregate, which decomposed into CaO and CO_2, resulting in a brighter appearance (i.e.,

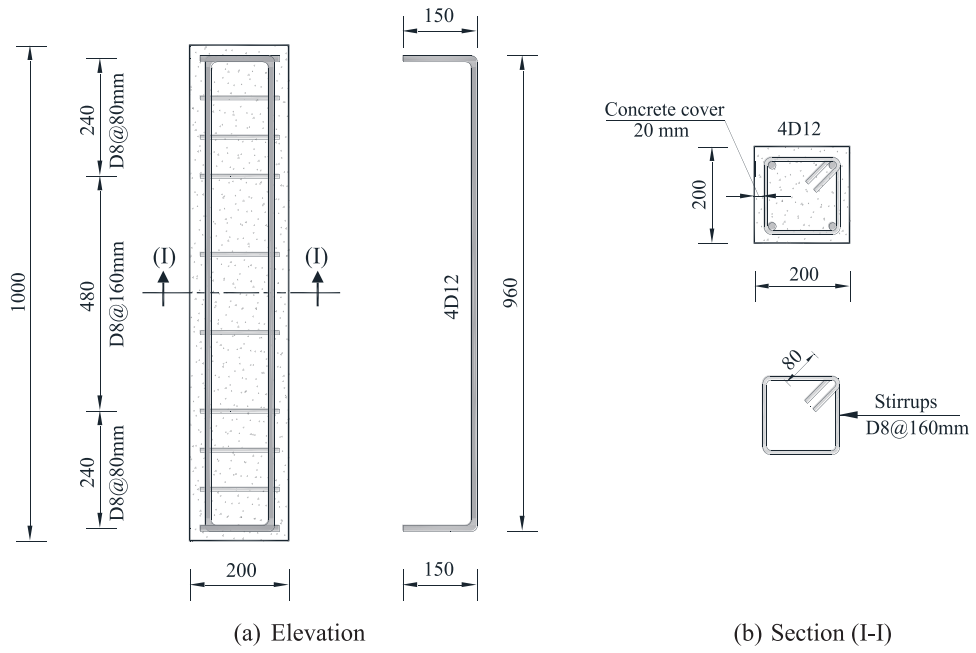


Fig. 3. Geometry and reinforcement details of the tested columns (All dimensions in mm).

Table 3
Description of the test matrix.

Group No.	Specimen ID	T (°C)	D (hr)	t_{SHCC} (mm)	Test conditions	Objectives
Control	$CC_{Amb-0-0}$	20 (Ambient)	0	0	non-damaged/non-repaired	Reference specimen.
Group I	$CC_{600-1-0}$	600	1	0	post-fire/non-repaired	Studying the effect of fire exposure duration.
	$CC_{600-2-0}$	600	2	0		
	$CC_{600-3-0}$	600	3	0		
Group II	$CC_{400-2-0}$	400	2	0		Studying the effect of temperature level.
	$CC_{800-2-0}$	800	2	0		
Group III	$CR_{600-1-20}$	600	1	20	post-fire/SHCC-repaired	Studying the effect of using SHCC jacket after exposure to different fire durations.
	$CR_{600-2-20}$	600	2	20		
	$CR_{600-3-20}$	600	3	20		
Group IV	$CR_{400-2-20}$	400	2	20		Studying the effect of using SHCC jacket after exposure to different temperature levels.
	$CR_{800-2-20}$	800	2	20		
Group V	$CR_{600-2-30}$	600	2	30		Studying the effect of SHCC thickness.
	$CR_{600-2-40}$	600	2	40		

T = temperature level; D = fire duration, t_{SHCC} = thickness of the SHCC jacket.



Fig. 4. Fire process.

the concrete color became a whitish grey instead of its normal grey) [69]. After the discoloration inspection, the depth of the fire-damaged near-surface concrete layer was determined using indirect Ultrasonic Pulse Velocity (UPV) testing in accordance with ACI 228.2R-13 [70–74]. The velocity of an ultrasonic wave travelling through the exterior layer of the column cross-section is measured during this test. The duration of

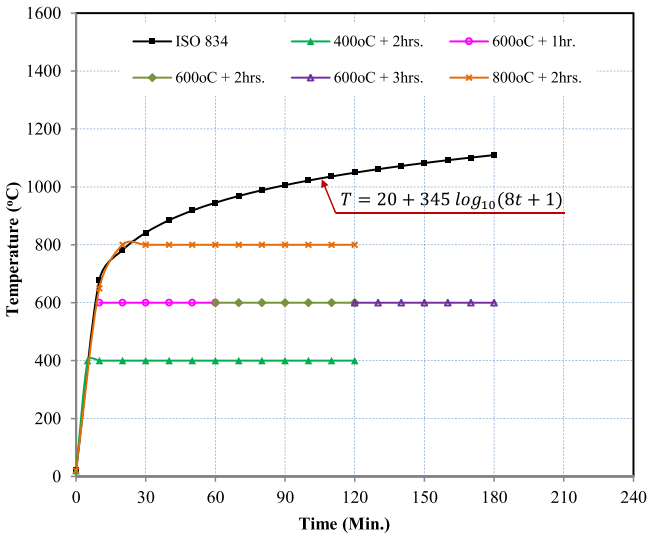


Fig. 5. The fire exposure history.

Table 4
Compressive strength value of all tested concrete cylinders.

T (°C)	D (hr)	Compressive strength (MPa)			
		Sample (1)	Sample (2)	Sample (3)	Average value
20 (Ambient)	0	20.20	20.80	21.70	20.90
400	2	14.90	14.20	14.10	14.40
600	1	15.68	13.52	14.51	14.57
600	2	11.00	11.50	9.81	10.77
600	3	8.30	7.10	6.29	7.23
800	2	6.00	5.50	5.60	5.70

T = temperature level; D = fire duration.

ultrasonic wave transmission is recorded at progressively increasing distances between the transducers. In the relationship between the distance (x) separating the transducers and the wave travel time (t), a characteristic change in the slope should occur at the abscissa marked x_o. This is the distance between the transducers for which the travel time of waves in the two paths is equal. Furthermore, V_d and V_s are the wave speeds in the damaged and the non-damaged concrete (see Fig. 8). The following formula may be used to calculate the thickness (d) of the damaged concrete layer [70].

$$d = \frac{x_o}{2}\sqrt{\frac{V_s - V_d}{V_s + V_d}} \tag{1}$$

It should be noted that the wave speed of the fire-damaged layer is lower than that of the non-damaged one. It was found that the extent of the depth of the damaged concrete layer ranged from 7 to 18 mm, depending on the fire exposure duration and temperature level, as listed in Table 5. At 400 °C, the surface layer is only affected and has minor crazing cracks and non-visible spalling, which can be classified as low damage level. However, when the specimens were exposed to around 600–800 °C, the damage degree was medium, and most of the concrete cover was affected. Moderate crazing cracks occurred due to the expansion and shrinkage of the concrete during heating and cooling, respectively, as well as surface spalling. This classification matches that described by Ingham and Tarada [75].

3.5. Repairing the post-fire columns using SHCC jacket

The repair process aims to restore both the original capacity and stiffness of the damaged columns, thereby improving their energy absorption capacity. To this end, the post-fire specimens were repaired by SHCC jackets after cooling down. The repair procedure was performed as follows: First, the whole columns' concrete cover (20 mm), including the deteriorated part determined based on the UPV test results, was carefully removed by grinding and hand-chiselling. It is worth mentioning that after the concrete cover removal, all columns had somewhat the same remaining cross-sectional dimensions. After that, pressurized air was used to remove the resultant dust and tiny particles, allowing an optimal bond between the SHCC jacket and the substrate concrete. Subsequently, the SHCC jacket was slightly reinforced by longitudinal bars of a ratio $(\rho_j = A_{sj}/A_{SHCC})$ of 0.6 % to alleviate any volumetric change, tied with two opposite U-shaped steel bars (6 mm in diameter) measuring 160 mm spacing between their centers (see Fig. 9), where A_{sj} is the area of steel reinforcement embedded inside SHCC and A_{SHCC} is the cross-sectional area of the SHCC jacket. Then, an epoxy resin bonding agent, Sikadur-32, was applied to the specimen's cleaned surfaces in order to enhance the bond between the concrete and the SHCC jacket. This step is necessary since the concrete surface may have some cracks due to fire exposure, which often affect the direct bonding of the SHCC. The epoxy resin can fill these cracks that SHCC can't, allowing for a better bond. As per the manufacturer's data sheet, the mechanical properties of the used epoxy agent were determined according to ASTM C881/C881M [76] (see Table 6). In addition, the chemical properties of the used Sikadur-32 meet the chemical resistance requirements of ASTM C881/C881M (Type II, Grade 2, Class B+C). After coating, the specimens were placed in a wooden formwork, where SHCC was poured with minor external vibration to reduce air voids. Finally, the specimens were covered with wet burlap to maintain moisture and then stored in the laboratory until testing.

In order to avoid local failure due to excessive stress concentration at the extreme ends of the tested columns, a length of 150 mm from the columns on both ends was strengthened with two layers of glass fiber reinforced polymer (GFRP) sheet glued using Sikadur-330. Table 6 summarizes the mechanical properties of the used adhesive epoxy, as specified by the manufacturer's data sheet. The steps of the repair process for RC columns damaged by fire are shown in Fig. 10.

3.6. Test setup and instrumentation

Fig. 11 shows the test setup and instrumentation for all tested specimens. A testing equipment with a 3000 kN capacity was used for all the axial compression tests. First, a load-controlled rate of 5 kN/s was applied to each specimen. Then, a displacement-controlled mode was used at a rate of 0.72 mm/min after the applied load surpassed 80 % of the predicted load capacity. Once the SHCC jacket ruptured, the loading operation was stopped. To precisely ensure the column's perpendicularity, a specially designed loading steel cap fastened with four bolts was used. Moreover, all specimens were capped with a thin layer of gypsum prior to testing to ensure a level contact surface for achieving perfect concentric loading on the column.

The developed deformations were captured using five linear variable differential transformers (LVDTs) of 100 mm stroke, designated as L1 to L5. Two of them (L1 and L2) were installed at the upper loading head to measure the total axial displacements. While L3 and L4 were mounted at the mid-height of the column to trace the developed hoop strains. In addition, another LVDT (L5) was positioned at the mid-height of the specimen to ensure that no buckling occurred during the test. Different electrical strain gauges were utilized to determine the resultant strains either in the longitudinal steel bars or the mid-height stirrups. A data acquisition unit was used to collect and store the results of strain gauges, LVDTs, and the load cell during testing.

4. Test results and discussions

The experimental results for all tested columns are discussed and

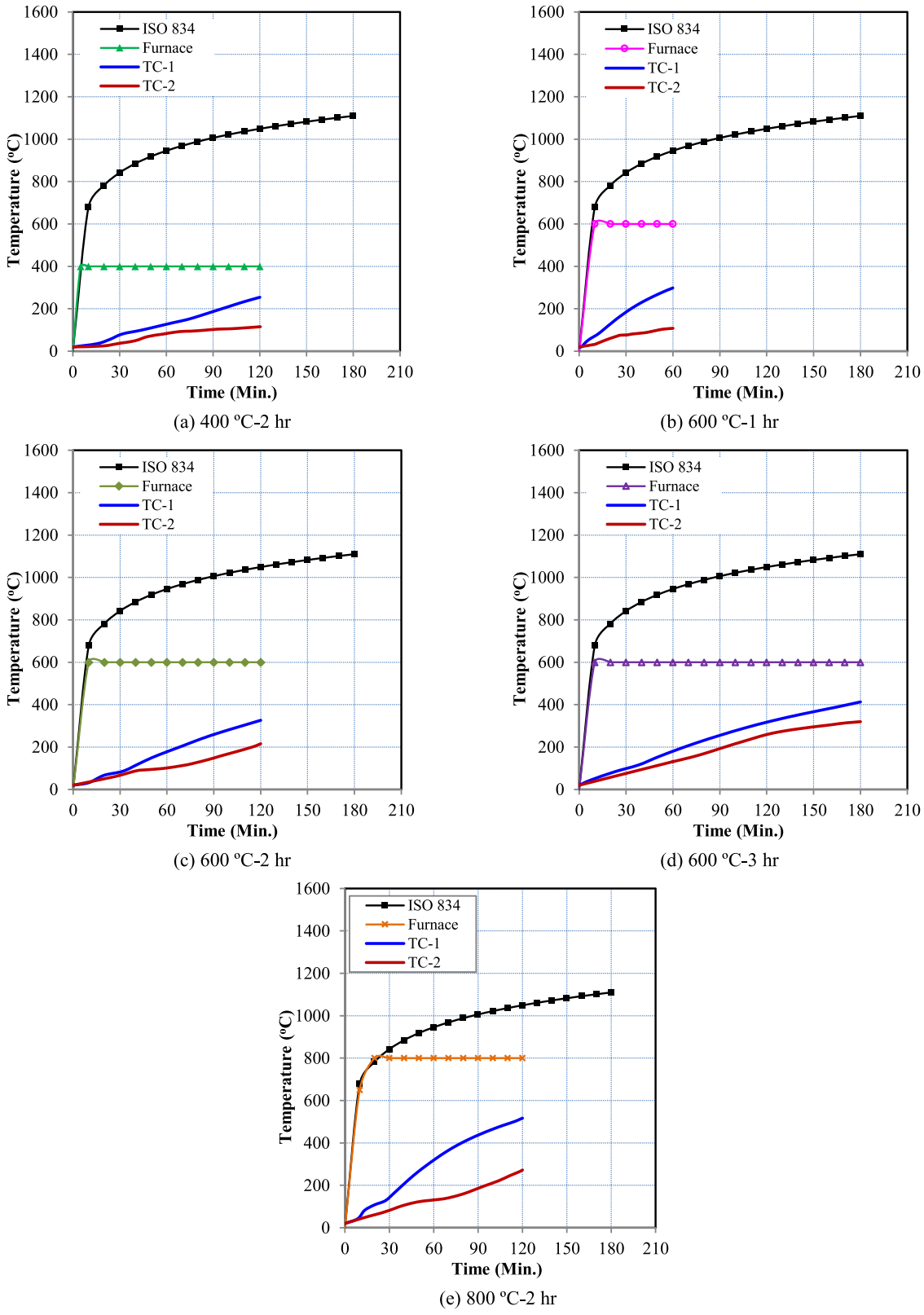


Fig. 6. Average temperature (T) versus time (t) curves for the specimens during the fire process.

analyzed to verify the efficiency of the adopted repair system (SHCC jacket) in enhancing the behavior of post-fire RC columns. These results include the mode of failure, load-displacement response, load-carrying capacity, stiffness, energy absorption, and strain analysis.

4.1. Mode of failure

In a similar manner, all specimens were tested up to failure under axial compression. For the reference specimen $CC_{Amb\text{-}0\text{-}0}$ (without fire damage), the failure was initiated by vertical hairline cracks that



Fig. 7. Specimens after fire exposure.

became visible at about 80 % of its ultimate strength. As expected, first along the corner due to the high stress concentration, and then all over the column surface. After that, as a result of pure axial compression, the mid-height concrete crushed suddenly, followed by explosive spalling with a loud booming noise. Consequently, steel rebars were found to be buckled in the region of failure, signifying a typical brittle mode of failure; see Fig. 12(a). Similar observation was also reported by Yaqub et al. [31,32]. It should be noted that the use of GFRP wraps for restricting column ends effectively prevented local failure at those ends, as was intended. For the post-fire specimens, the crack pattern was similar to those of the reference column ($CC_{Amb\text{-}0\text{–}0}$) in shape and location, but a more gradual failure was noticed, as seen in Figs. 12(b) to 12(f). This result, which is consistent with the findings of Abo-Zaid et al. [77], may be attributed to the formation of temperature-induced cracks. The concrete cover disintegration became more obvious for the severely damaged columns ($CC_{600\text{–}3\text{-}0}$ and $CC_{800\text{–}2\text{-}0}$), which is believed to be caused by the development of internal stresses associated with increased temperature, as stated by Al-Nimry and Ghanem [38]. Consequently, the peak loads were drastically decreased owing to the extra-formation of thermal cracks.

For the post-fire/SHCC repaired specimens, a different failure mode compared to the non-repaired specimens (both non-damaged and post-fire) was induced, as shown in Figs. 12(g) to 12(m). Three stages made up the whole loading process for the repaired specimens which was in line with Liu et al. [7]. Initially, the SHCC jacket experienced tensile stress as the concrete column expanded laterally. This resulted in small visible hair cracks on the surface at about 50 % of the peak load, as well as some intermittent sounds produced by the PP fibers inside the SHCC matrix. Then, in the second stage, prior to the peak load, a large crack was formed first near the column corner and then all over its surface, alongside the frequently loud noise resulting from tensile rupture of PP fibers. In the third stage, as the crack propagated and widened; the SHCC jacket reached its ultimate strain, buckling of the bars became obvious, and the column eventually failed. The same failure mode was also observed in previous studies [78–81] for SHCC-strengthened RC columns. After the removal of the SHCC cover, inspection of the failed columns revealed that the lateral tie was also slightly opened outwards under the large lateral pressure exerted by the concrete core. A more gradual failure without severe spalling could be achieved by the SHCC jacket due to its better deformation compatibility with the concrete column. Moreover, the failure modes showed that the SHCC jacket remained structurally intact during the compression test, i.e., part of the concrete was still attached to the SHCC, indicating that the SHCC and the fire-damaged concrete did not show any signs of debonding or delamination, as predicted.

4.2. Load-carrying capacity

The compressive strength of concrete when exposed to fire, irrespective of the mix proportions, decreases at a faster rate as the temperature increases. The cement paste shrinks, and the aggregate expands at high temperatures, which shows a considerable degradation in the materials' composition. In this study, the compressive residual strength of the used concrete cylinders was 70 %, 52 %, and 35 % at 600 °C for 1, 2, and 3 hrs., respectively. Moreover, it was observed that the rate of reduction increased significantly when the temperature levels rose within the range of 400 °C to 800 °C for 2 hrs. The resulting compressive residual strength of the cylinders was found to be 69 % (at 400 °C) and 27 % (at 800 °C) compared to the cylinder strength at ambient temperature. These results somewhat correspond to the findings established in the previous research/standards [6,63,77]. Consequently, this reduction in concrete strength had a direct impact on the axial capacity and stiffness of the post-fire columns.

The main test results for all specimens, including their load-carrying capacity (i.e., peak load = P_u), secant stiffness, energy absorption, and ultimate displacement (Δ_u) are summarized in Table 7. The load-carrying capacity of specimens $CC_{600\text{–}1\text{-}0}$, $CC_{600\text{–}2\text{-}0}$, and $CC_{600\text{–}3\text{-}0}$ experienced severe degradation from 928 kN ($CC_{Amb\text{-}0\text{–}0}$) to 673, 473, and 335 kN, respectively. This translates to 27 %, 49 %, and 64 % loss of capacity after exposure to 600 °C for 1, 2, and 3 hrs. The specimens $CC_{400\text{–}2\text{-}0}$, $CC_{800\text{–}2\text{-}0}$ had reductions in their capacity of 23 % and 63 %,

Table 5
The depth of damaged layers based on indirect UPV.

Specimen ID	V_d (m/s)	V_s (m/s)	x_o (mm)	d (mm)
$CR_{600-1-20}$	2500	3600	55.32	12
$CR_{600-2-20}$	1700	3480	53.27	16
$CR_{600-3-20}$	1200	3300	49.60	17
$CR_{400-2-20}$	2800	3670	40.20	7
$CR_{800-2-20}$	1400	3700	55.00	18
$CR_{600-2-30}$	1650	3480	53.00	16
$CR_{600-2-40}$	1710	3510	52.80	16

V_d and V_s are the wave speeds in the damaged and the non-damaged concrete, x_o is the distance at which the travel times for the two paths are equal, d is the thickness of the damaged concrete layer.

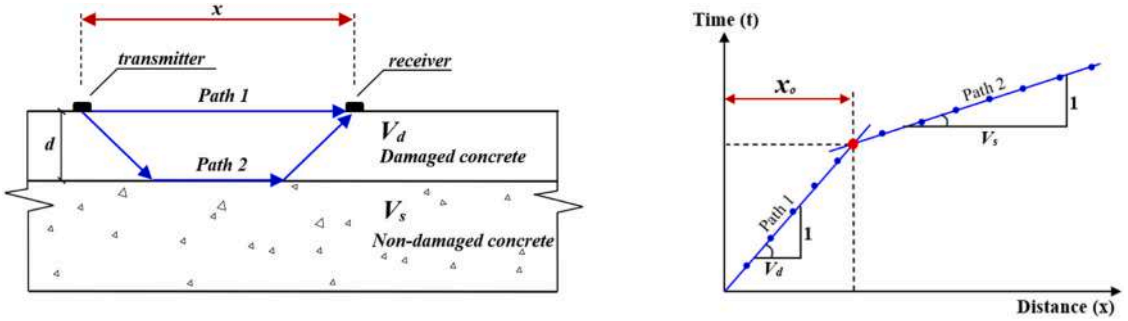


Fig. 8. Scheme of UPV measurement (according to ACI 228.2R-13 [70]).

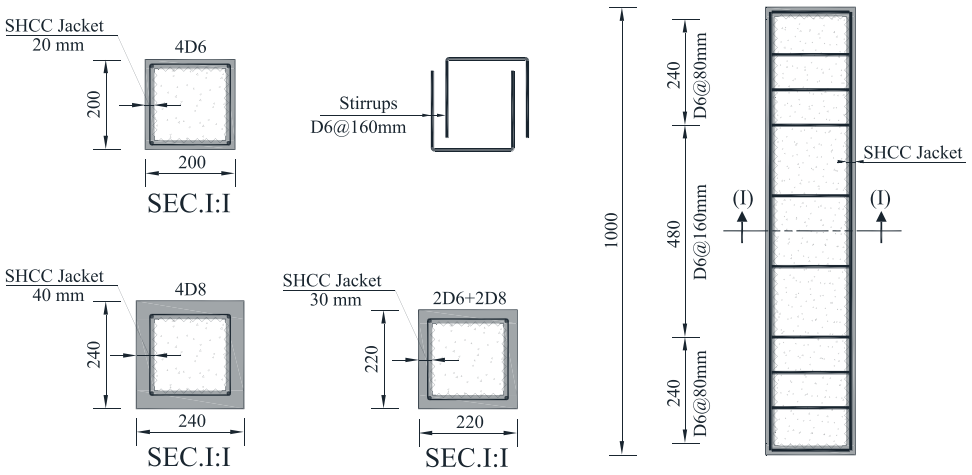


Fig. 9. Details of SHCC jackets (All dimensions in mm).

Table 6
Properties of the used epoxy resins.

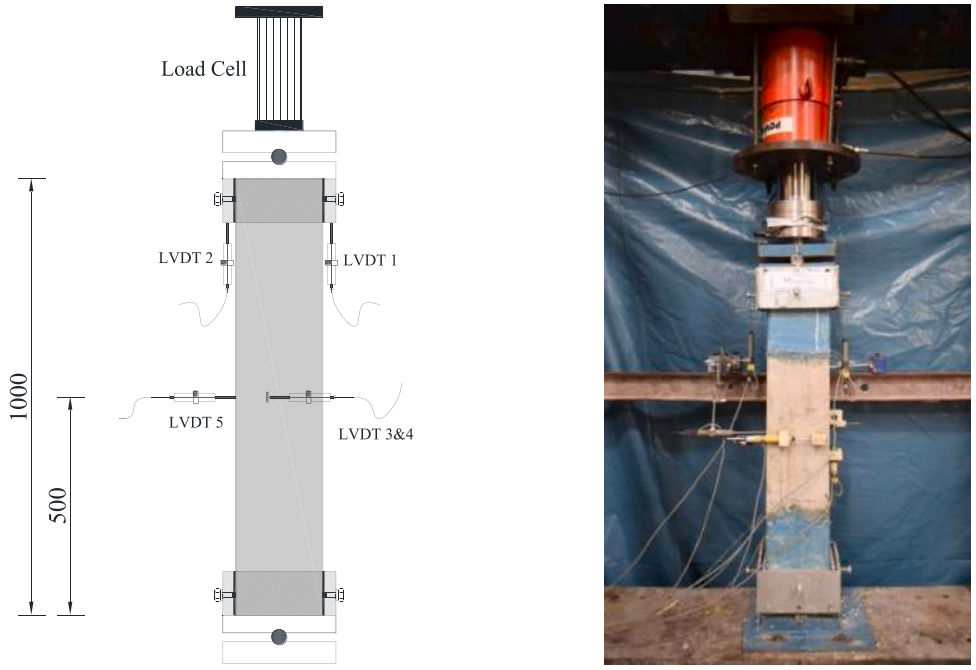
Material	Density @ 20 °C (kg/l)	Compressive strength (MPa)	Flexural strength (MPa)	Tensile strength (MPa)	Bond strength to concrete (MPa)	Bond strength to steel (MPa)
Sikadur−32	1.4	50 −60	30 −35	18 −20	2.5 −3	18 −20
Sikadur−330	1.30 ± 0.1	—	—	30	> 4	—



(a) Reinforcement cage (b) Painting the adhesive epoxy (c) Casting the SHCC jacket

(d) Repaired column (e) GFRP wrapping (f) Final column before testing

Fig. 10. The main steps for repairing the post-fire RC columns.



(a) Schematic details (b) Lab view

Fig. 11. Test setup (All dimensions in mm).

respectively, when exposed to 400 °C and 800 °C for 2 hrs, compared to the reference non-damaged specimen ($CC_{Amb\text{-}0\text{–}0}$). The loss of the concrete's bond with the internal reinforcements, the formation of microcracks, and the concrete's disintegration are the main reasons for this reduction.

The efficiency of using the SHCC jacket as a repair system is shown in Fig. 13. In this figure, "inherent" signifies the ratio of the strength of post-fire specimens to the strength of non-damaged specimen (in percent); "lost" shows the ratio of the lost strength of post-fire specimens to the strength of non-damaged specimen (in percent); and "gained" indicates the ratio of the gained strength of SHCC-repaired specimens to the strength of non-damaged specimen (in percent). Upon applying the SHCC jacket to the post-fire specimens, significant restoration in the load-carrying capacities was attained. As observed in Table 7, specimens $CR_{600\text{–}1\text{-}20}$, $CR_{600\text{–}2\text{-}20}$, and $CR_{600\text{–}3\text{-}20}$ (group III) attained a load-carrying capacity of 1378 kN, 1284 kN, and 1082 kN, respectively. This turns to 48 %, 38 %, and 17 % increase in P_u as compared to the non-damaged specimen $CC_{Amb\text{-}0\text{–}0}$. Similarly, specimens $CR_{400\text{–}2\text{-}20}$ and $CR_{800\text{–}2\text{-}20}$ (group IV) had ultimate loads of 1400 kN and 1181 kN, respectively, which achieved a 51 % and 27 % increment in load-carrying capacity when compared to the non-damaged specimen $CC_{Amb\text{-}0\text{–}0}$. This increase is attributed to the fact that columns expand laterally when subjected to an axial load, causing tensile stress in the SHCC jacket, which in turn confines the concrete, hence improving the load-carrying capacity of post-fire columns. It is worth mentioning that the higher the damage level, the greater the confinement generated by the SHCC jacket.

As far as SHCC thickness is concerned, logically, the increase in SHCC thickness resulted in a better contribution of SHCC to the axial capacity of RC columns. Compared to specimen $CR_{600\text{–}2\text{-}20}$, with a 20 mm SHCC jacket thickness, specimens $CR_{600\text{–}2\text{-}30}$ and $CR_{600\text{–}2\text{-}40}$ failed at an ultimate load of 1807 kN and 2326 kN, which represented a gain in P_u of 41 % and 81 %, respectively. This is because the expansion of RC columns is limited due to the extra-confinement effect supplied by SHCC, and increasing the thickness of the SHCC jacket brings stronger confinement to post-fire columns. In brief, it can be concluded (as shown in Fig. 13) that the proposed repair technique could restore the post-fire columns' strength back to the original level as the non-damaged reference column.

4.3. Analysis of the load-axial displacement curves

Fig. 14 shows a comparison of the specimens' load-axial displacement curves under different studied parameters. It can be noticed that the load-displacement curve for the reference specimen $CC_{Amb\text{-}0\text{–}0}$ almost followed a straight line till reaching the ultimate load and then unexpectedly dropped. However, the load-axial displacement curves of RC columns exhibit a flattening trend following fire exposure, and their peak values clearly reduced and leaned towards the right side compared to its counterpart at ambient temperature. As a result, the axial stiffness of RC columns decreased sharply. It may be attributed to the reality that concrete deteriorates and loses strength and stiffness when exposed to high temperatures. This occurs due to the interaction of several physical, chemical, and mechanical processes, including water and vapor advection, dehydration, cracking, and spalling. In contrast, all other SHCC-repaired specimens achieved enhanced post-peak softening behaviors, representing the effectiveness of the adopted repairing system in enhancing the ductility as well as the load-displacement response of these specimens. This could be attributed to the fact that SHCC jacket provided significant confinement to microcracks in post-fire RC columns.

4.3.1. Stiffness

In any RC building, loads are distributed based on the stiffness of the structural members. As a result, the repaired RC building should regain both capacity and stiffness to the original level of the non-damaged members. The secant stiffness (K) of the specimens was determined through dividing the measured ultimate axial load by its counterpart axial displacement [31]. From Table 7, it can be observed that the secant stiffness of the post-fire RC columns was inversely proportionate to the fire exposure duration or temperature level. The reductions in secant stiffness were up to 33 %, 62 %, and 76 % after exposure to 600 ºC for 1, 2, and 3 hrs., respectively. It is noteworthy to mention that specimen $CC_{800\text{–}2\text{-}0}$, which was exposed to 800 °C for 2 hrs., recorded the lowest stiffness value (44 kN/mm). That was due to the fact that, on heating, the loss of moisture and the formation of internal micro-cracking cause concrete's porosity to rise, which ultimately leads to a loss of stiffness.

An intriguing result is that applying the SHCC jacketing technique



Fig. 12. Cracking patterns and failure of all tested specimens.

can significantly improve the secant stiffness of the post-fire RC columns. As shown in Fig. 15, the repaired specimens not only restored the stiffness of the reference non-damaged specimen ($CC_{Amb-0-0}$) but, in several cases, exceeded it. The secant stiffness for specimens with a 20 mm SHCC jacket thickness ranged from 239 to 284 kN/mm, which was almost higher than that for specimen $CC_{Amb-0-0}$ (238 kN/mm). Also, the secant stiffness values were enhanced as the thickness of the SHCC jacket increased. For example, the secant stiffness was greater for specimen $CR_{600-2-40}$ (331 kN/mm) than that for specimen $CR_{600-2-30}$ (275 kN/mm), which was subsequently higher than that for specimen $CR_{600-2-20}$ (269 kN/mm). This observation contrasts with the experimental findings of Yaqub et al. [31], in which the post-fire RC columns strengthened with CFRP sheets did not exhibit enhanced secant stiffnesses. The different findings noted in this research can be explained by the fact that the deformation compatibility between the SHCC and the concrete core activates the repairing jacket in the early loading stage, which in turn restores the stiffness of fire-damaged RC columns.

4.3.2. Energy absorption

Even now, there is an issue of contention in the engineering field on how to precisely define ductility. The ductility concept refers to the ability of structural elements to carry internal forces through substantial deformations prior to failure. Energy absorption capacity (E) is one of the most important ductility indicators of RC elements. In order to determine the energy absorption in this study, the area under the load-axial displacement curve was integrated up to the post-peak load, which is 85 % of the ultimate load [82]. It can be noted that the energy absorption capacity of the columns after exposure to 600 ºC for 1, 2, and 3 hrs. decreased by around 16–40 %. This reduction was 15 % and 45 % when exposed to 400 °C and 800 °C for 2 hrs.

As stated in Table 7, the repaired specimens showed a considerable enhancement in their energy absorption capacities compared to the reference non-damaged specimen ($CC_{Amb-0-0}$). The SHCC-repaired specimens, which had been previously exposed to 600 ºC for 1, 2, and 3 hrs., respectively, showed 164 %, 137 %, and 73 % greater energy absorption, respectively, than the specimen $CC_{Amb-0-0}$. In addition, this increase ranged from 171–106 % for the repaired specimens after exposure to 400 °C and 800 °C for 2 hrs. Furthermore, this enhancement became more pronounced with the increase in the jacket's thickness. The maximum increase in energy absorption (635 %) was recorded for specimen $CR_{600-2-40}$, repaired by a 40 mm SHCC jacket. This improvement in energy absorption is caused by two reasons: (1) the SHCC jacket's ability to improve ultimate capacity; and (2) the repaired specimens exhibit greater ductility after being confined by the SHCC

Table 7
Experimental results.

Group No.	Specimen ID	Ultimate axial load			Axial displacement		Stiffness			Energy absorption		
		P_u (kN)	% Change		Δ_u (mm)	$\Delta_{0.85}$ (mm)	K (kN/mm)	% Change		E (kN.mm)	% Change	
			a	b				a	b		a	b
Control	$CC_{Amb-0-0}$	928	—	—	3.90	4.26	238	—	—	2153	—	—
Group I	$CC_{600-1-0}$	673	27	—	4.24	4.58	159	33	—	1810	16	—
	$CC_{600-2-0}$	473	49	—	5.19	5.74	91	62	—	1454	32	—
	$CC_{600-3-0}$	335	64	—	5.75	6.08	58	76	—	1285	40	—
Group II	$CC_{400-2-0}$	711	23	—	4.30	4.72	165	31	—	1820	15	—
	$CC_{800-2-0}$	339	63	—	7.69	8.04	44	81	—	1191	45	—
Group III	$CR_{600-1-20}$	1378	—	48	4.85	6.44	284	—	19	5682	—	164
	$CR_{600-2-20}$	1284	—	38	4.77	6.76	269	—	13	5109	—	137
	$CR_{600-3-20}$	1082	—	17	4.52	5.67	239	—	0	3719	—	73
Group IV	$CR_{400-2-20}$	1400	—	51	5.00	6.70	280	—	18	5827	—	171
	$CR_{800-2-20}$	1181	—	27	4.73	5.65	250	—	5	4433	—	106
Group V	$CR_{600-2-30}$	1807	—	95	6.58	9.02	275	—	16	10330	—	380
	$CR_{600-2-40}$	2326	—	151	7.03	9.79	331	—	39	15832	—	635

P_u = load-carrying capacity, $P_{u,0}$ = load-carrying capacity of the control specimen; Δ_u = ultimate axial displacement, $\Delta_{0.85}$ = axial displacement corresponding to 85 % of ultimate load after the peak; K = secant stiffness, K_0 = secant stiffness of the control specimen; E = energy absorption, E_0 = energy absorption of the control specimen; a = the percentage of post-fire damage relative to the non-damaged reference column, b = the improvement due to the SHCC jacket relative to the non-damaged reference column.

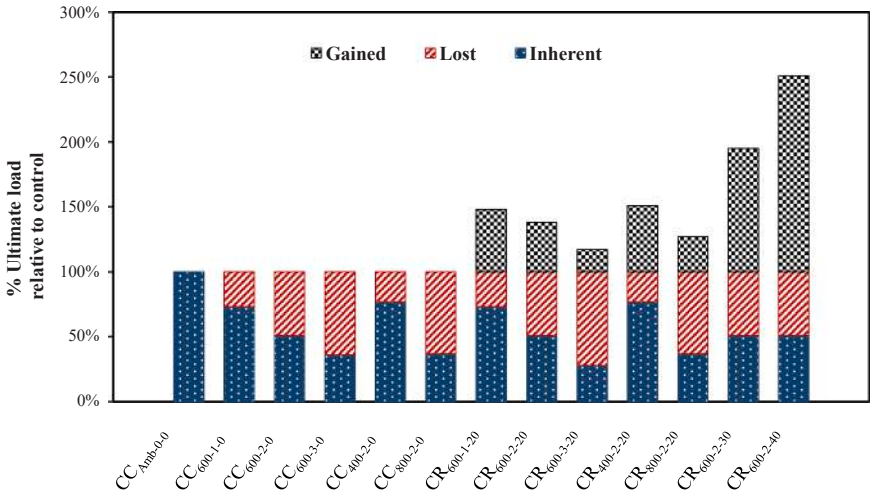


Fig. 13. Ability of SHCC jacket to restore the axial capacity of the post-fire columns.

jacket, which increases ultimate displacement (see Fig. 14). So, considering these outcomes, it was clear that the suggested SHCC repair system significantly improved the ductility behavior of the post-fire columns.

4.4. Lateral strains

As explained above in Section 3.6, the mean lateral (hoop) displacements at the column's mid-height were traced (from zero loading up to the ultimate load) and transformed into an average lateral strain over the LVDT measurement points (see Fig. 11). The axial load against lateral strains at the outer surface for all non-damaged, post-fire, and SHCC-repaired columns are shown in Fig. 16. All the load-strain curves exhibited similar trends, initially showing a tendency towards semi-linearity, then gradually decreasing in slope as the loads increased until reaching the peak load. It can be observed that, when the fire exposure time or temperature level increased, the slope of the curves decreased, indicating that the most severely damaged specimens had higher lateral strains under the same loading level, which is in line with the results of Song et al. [83]. Such large strains may be ascribed to the pre-existing defects such as micro-cracks, reduced stiffness of the concrete after fire exposure, and deterioration of the bond between the reinforcing steel and the concrete.

In contrast, applying the SHCC jacket repair system resulted in less deformation ability at the same loading level. In control and post-fire specimens without repair, the strain in the lateral direction reached the ultimate tensile strain of concrete at a relatively lower axial strain. However, in SHCC-repaired specimens, the SHCC jacket successfully enhanced the specimen's ability to sustain higher axial and lateral strains. Another point to note is that the greater the confinement provided by the larger thickness of the SHCC jacket, the higher the slope before the peak load. Consequently, specimen $CR_{600-2-40}$ exhibited lower hoop strains under the same loading level compared to the counterpart specimen $CR_{600-2-20}$, repaired by a 20 mm SHCC jacket.

5. Numerical simulation

A three-dimensional (3D) non-linear finite element (FE) model was developed using ABAQUS software [84] and then validated against the experimental outcomes. The numerical study was intended to offer reliable predictions of the behavior of fire-damaged columns repaired with SHCC. The development of the FE models is described in the

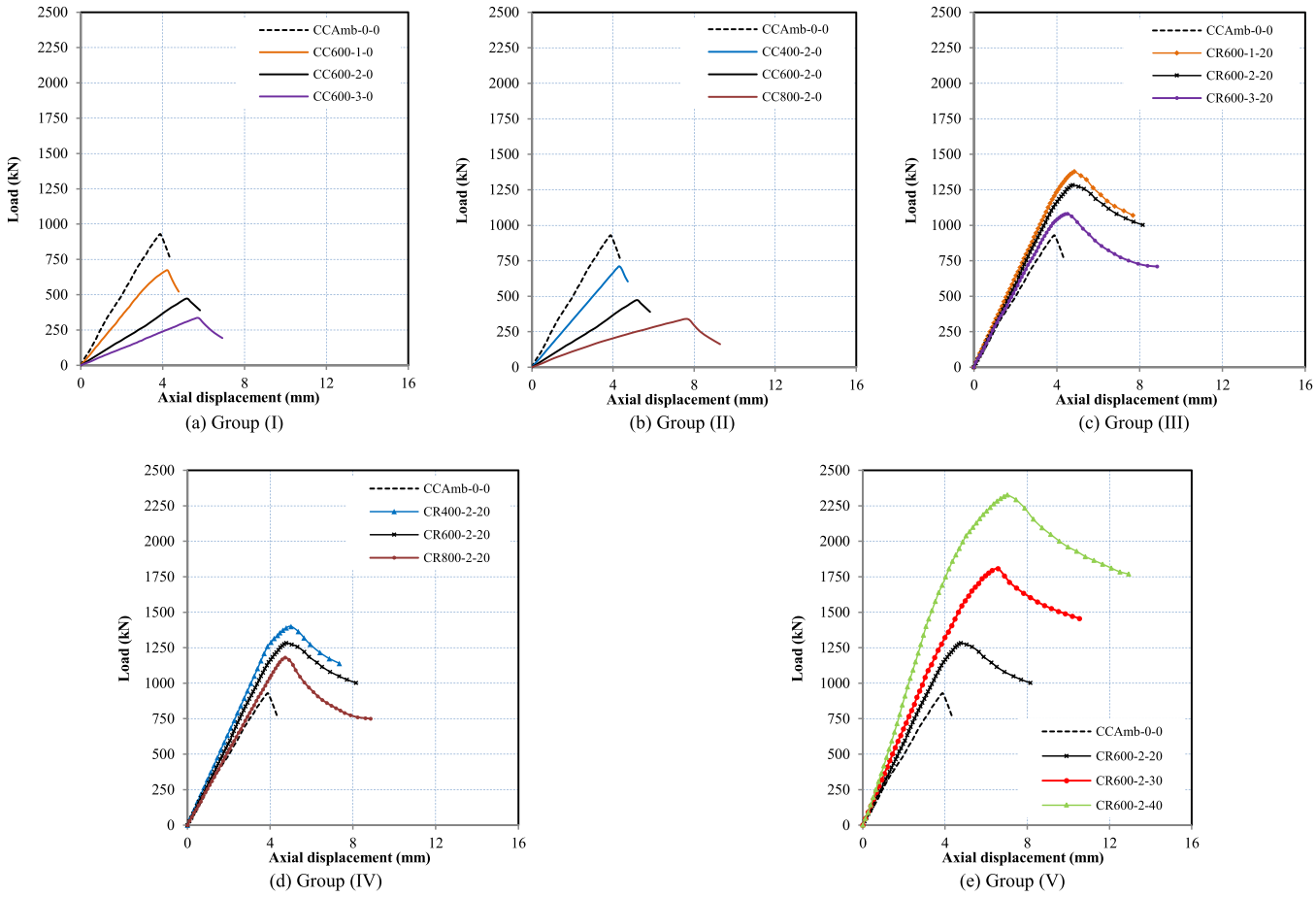


Fig. 14. Load-axial displacement relationships for the tested specimens.

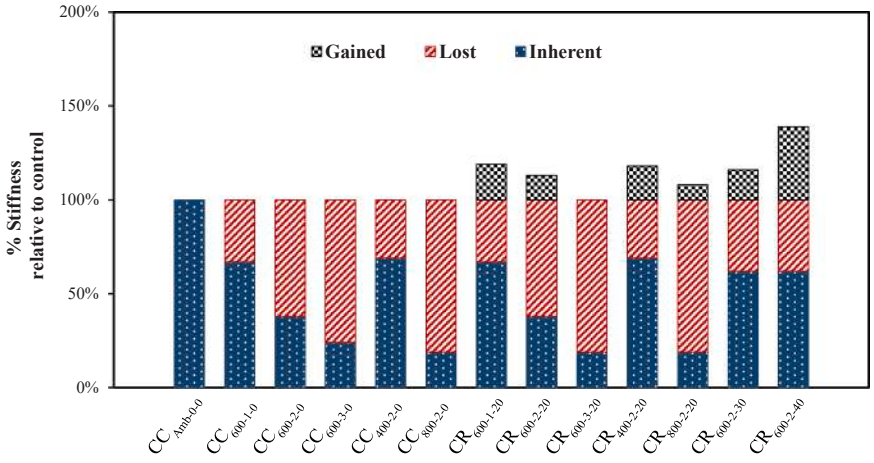


Fig. 15. Ability of SHCC jacket to restore the stiffness of the post-fire columns.

following sub-sections:

5.1. Model built-up

In the current study, the model carefully depicted the different elements, as presented in Fig. 17. Normal strength concrete (NSC), fastening bolts, upper and lower steel caps, and SHCC jackets have been simulated using eight-node hexagonal linear reduced integration solid elements (C3D8R). In this manner, the three-dimensional body and structural performance of these components were well represented. Main longitudinal reinforcing steel bars, SHCC-embedded reinforcement, and transverse steel reinforcement in the concrete core as well as in the SHCC jacket have been simulated by two-node linear 3D truss elements (T3D2) in order to represent their function in both tension stresses and compression counterparts. In the experimental program, top and bottom GFRP sheets were used to prevent undesired failure in these regions. These sheets were simulated using a four-node shell element with reduced integration (S4R) in order to represent their thin, plate-like properties. Based on mesh sensitivity analysis, a mesh size of 25 mm was selected to achieve a satisfactory balance between numerical efficiency

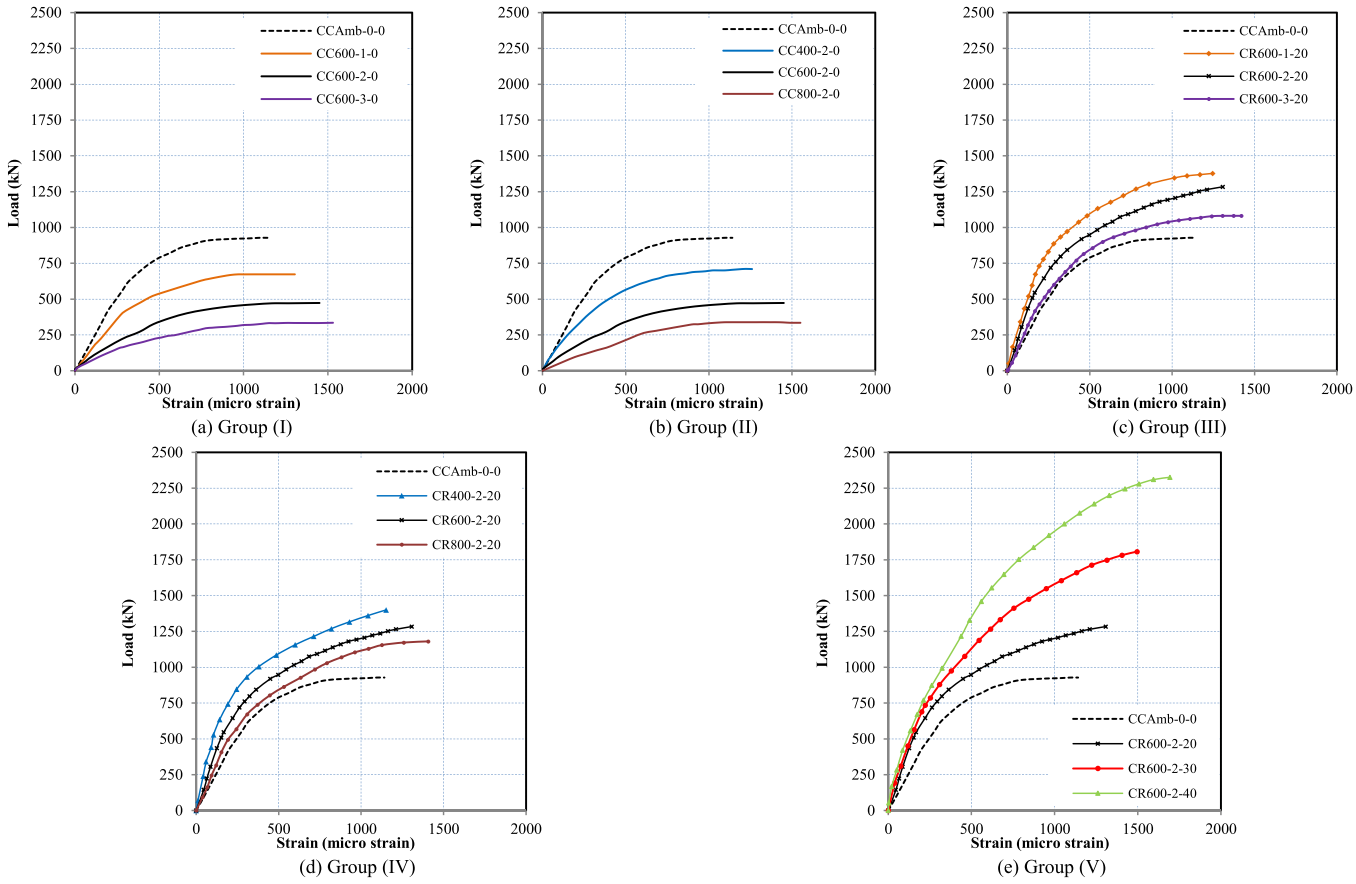


Fig. 16. Load-lateral strains relationships for the tested specimens.

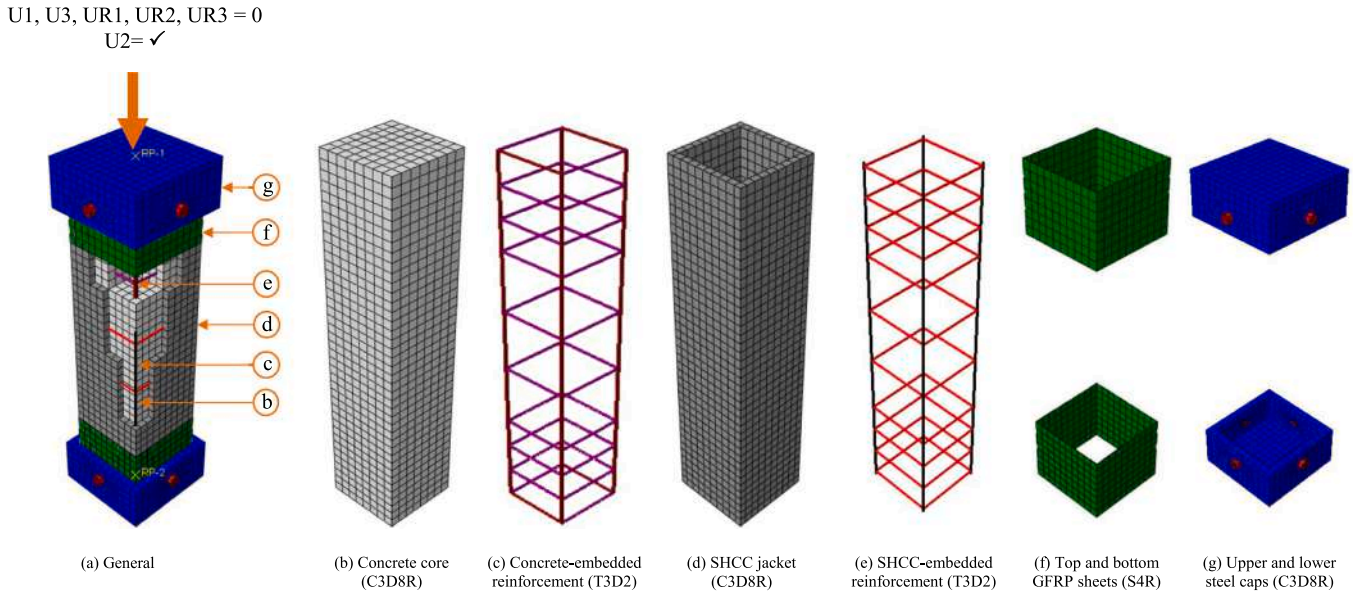


Fig. 17. Numerical model of column $CR_{600-1-20}$, boundary conditions, and used elements.

and job-time.

5.2. Boundary conditions and loading strategy

The numerical models used a comprehensive approach in order to simulate the interactions between the various elements involved in the experimental study. Embedded region constraints were applied in order to simulate the interaction between the concrete core, longitudinal reinforcing steel, SHCC-embedded reinforcement, transverse steel reinforcements, and the SHCC jacket. In this method, any concrete element acts as the host region, and any steel element acts as an embedded one. In addition, the simulation utilized a hard contact approach that allows for separation in the normal direction and incorporates a penalty friction coefficient in the tangential direction. This

approach, known as ABAQUS's surface-to-surface contact algorithm, was employed to model the interaction between the upper/lower steel caps, GFRP sheets, and the surface of the tested columns. The same approach (hard contact/surface-to-surface allow separation) was employed to simulate the interaction between the SHCC jacket and the core of the original column. The arrangement of these components is depicted in Fig. 18.

Moreover, three steps for loading arrangement in the numerical models were employed, as shown in Fig. 18. The first step was used to simulate the application of the temperature effect on the inner RC column (concrete core) according to the experimental program presented in Table 3. The application of the temperature effect was simulated with respect to both temperature degree and fire duration (fire exposure history), as shown in Fig. 5. The second step was prepared to simulate tightening the fastening bolts in the upper and lower steel caps in order to confine the tested column in loading regions. Finally, an axial loading strategy was presented in the center line of the steel cap, as shown in step 3 in Fig. 18.

Fig. 19 presents the performance of the cohesive-damaged interaction used in the modeling process. The performance of this interaction simulated all characteristics of adhesive epoxy that contact SHCC jackets with columns. It is worth mentioning that three distinct phases characterize how the interaction progresses: the first defines the shear stiffness of the interaction, the second indicates the point where maximum shear stress is reached on the surface, and the third details the interaction's behavior after the maximum stress has been surpassed.

5.3. Fire methodology

In the simulation of the experimental program, three main stages of fire exposure and jacketing for the columns were involved, as follows:

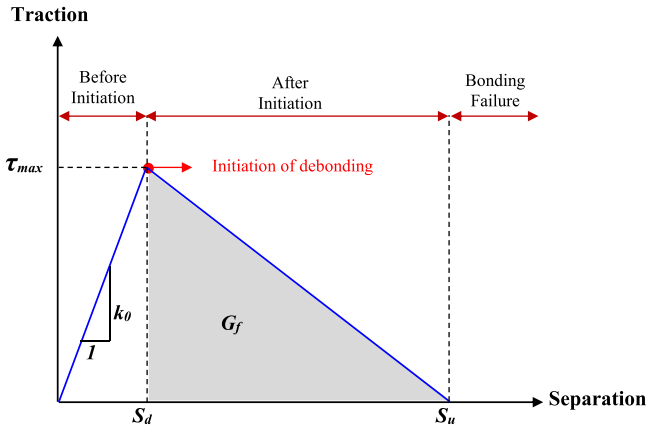
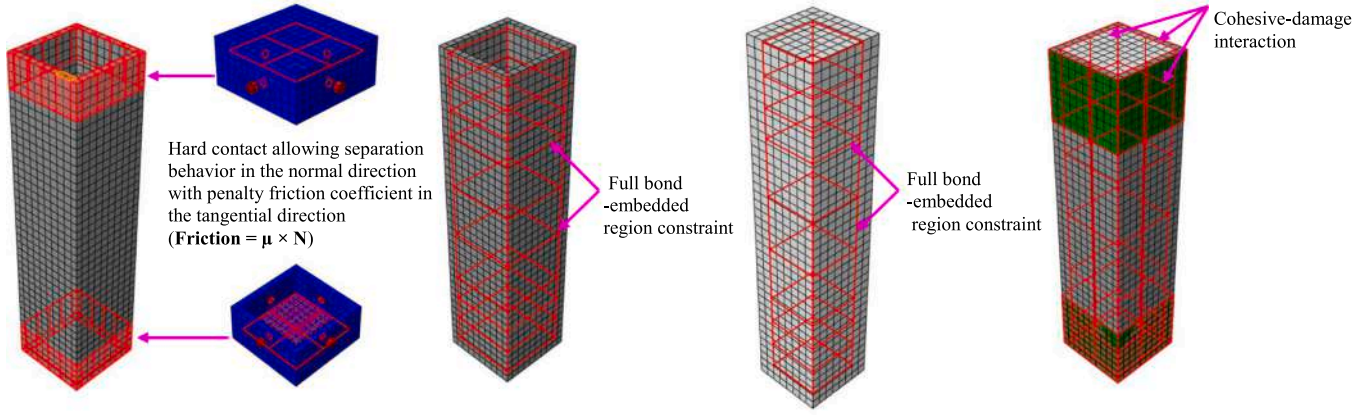


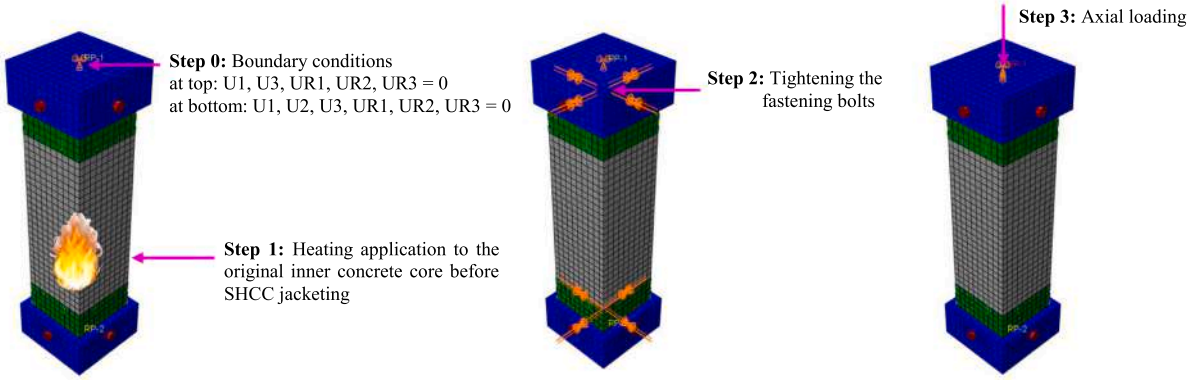
Fig. 19. Cohesive-damage interaction behavior.

1. Heating application with different designed temperatures to the original column without any jacketing, as mentioned previously in Section 3.3.
2. Removing the concrete cover of the columns after the heating, as described in Section 3.4.
3. Coating with adhesive material and covering with an SHCC jacket with the required thicknesses according to the experimental program, as detailed in Section 3.5. It is worth mentioning that after applying the SHCC jacket, the columns were not exposed to fire again. The thin SHCC jackets were employed in order to improve the performance of such heated columns.

The previous steps were modeled sequentially to ensure that the numerical simulation accurately reflects the experimental procedures.



(a) Interactions between different elements



(b) Steps of loading

Fig. 18. Interactions between different elements and steps of loading.

5.3.1. Thermal properties

For NSC, the thermal properties (specific heat capacity, density, thermal conductivity, and so on) were developed in accordance with EN 1992–1-2 [63], whereas for steel reinforcement, the thermal properties and reduction factor were derived from EN 1993–1-2 [85].

The thermal strains $\varepsilon_c(\theta)$ for concrete were calculated through the following equations:

$$\varepsilon_c(\theta) = -1.2\times10^{-4} + 6\times10^{-6}\theta + 1.4\times10^{-11}\theta^3 \quad for \quad 20^\circ C \le \theta \le 805^\circ C \tag{2}$$

$$\varepsilon_c(\theta) = 12\times10^{-3} \quad for \quad 805^\circ C < \theta \le 1200^\circ C \tag{3}$$

Where θ is the concrete temperature (°C).

The specific heat $c_p(\theta)$ of dry concrete ($u = 0\%$) may be determined from the following:

$$c_p(\theta) = 900 \quad (J/kgK) \quad for \quad 20^\circ C \le \theta \le 100^\circ C \tag{4}$$

$$c_p(\theta) = 900 + (\theta - 100) \ (J/kgK) \quad for \quad 100^\circ C < \theta \le 200^\circ C \tag{5}$$

$$c_p(\theta) = 1000 + (\theta - 200)/2 (J/kgK) \quad for \quad 200^\circ C < \theta \le 400^\circ C \tag{6}$$

$$c_p(\theta) = 1100 (J/kgK) \quad for \quad 400^\circ C < \theta \le 1200^\circ C \tag{7}$$

The variation of density with temperature is influenced by water loss and is defined as

$$\rho(\theta) = \rho(20^\circ C) \quad for \quad 20^\circ C \le \theta \le 115^\circ C \tag{8}$$

$$\rho(\theta) = \rho(20^\circ C) \times (1 - 0.02 \ (\theta - 115)/85) \quad for \quad 115^\circ C < \theta \le 200^\circ C \tag{9}$$

$$\rho(\theta) = \rho(20^\circ C) \times (0.98 - 0.03 \ (\theta - 200)/200) \ for \ 200^\circ C < \theta \le 400^\circ C \tag{10}$$

$$\rho(\theta) = \rho(20^\circ C) \times (0.95 - 0.07 \ (\theta - 400)/800) \ for \ 400^\circ C < \theta \le 1200^\circ C \tag{11}$$

The upper limit of thermal conductivity λ_c of normal strength concrete may be determined from:

$$\lambda_c = 2 - 0.2451 \ (\theta/100) + 0.0107 (\theta/100)^2 \ W/mK \ for \ 20^\circ C \le \theta \le 1200^\circ C \tag{12}$$

The lower limit of thermal conductivity λ_c of normal strength concrete may be determined from:

$$\lambda_c = 1.36 - 0.136 \ (\theta/100) + 0.0057 (\theta/100)^2 \ W/mK \ for \ 20^\circ C \le \theta \le 1200^\circ C \tag{13}$$

5.3.2. Heat transfer modeling

During fire process, the column experiences heat transmission via radiation and convection. In FE method, steel and concrete's thermal characteristics, including specific heat, thermal conductivity, and density, play a significant role in the temperature distribution. The four edges of the column were considered exposed to the fire exposure history (mentioned previously in Section 3.3). According to EN 1991–1-2 [86], the convective heat transfer coefficient for the surface exposed to fire was assumed to be $25 W/m^2K$, and the thermal model included radiation heat transfer with a concrete emissivity $\varepsilon = 0.7$. The temperature distribution in the column cross-section is the outcome of the heat transfer model.

5.4. Material constitutive modeling

For the nonlinear part, the damaged plasticity model was used, with parameters derived from previous research [87,88]. The stress-strain relationships for both NSC and SHCC were idealized according to the model presented by Baraghith et al. [46] and Emara et al. [89]. For SHCC, it had an idealized relationship with an average cylinder compressive strength of 67.90 MPa and a uniaxial tensile strength of 8.48 MPa, as mentioned in Section 3. The NSC model was idealized to include exposure duration (1, 2, or 3 hrs.) and temperature level (400 ºC, 600 ºC, or 800 ºC). Two models were used to simulate the various steel members: the first was elastic-plastic performance to simulate all reinforcing steel. The other one was elastic performance to model the loading steel caps.

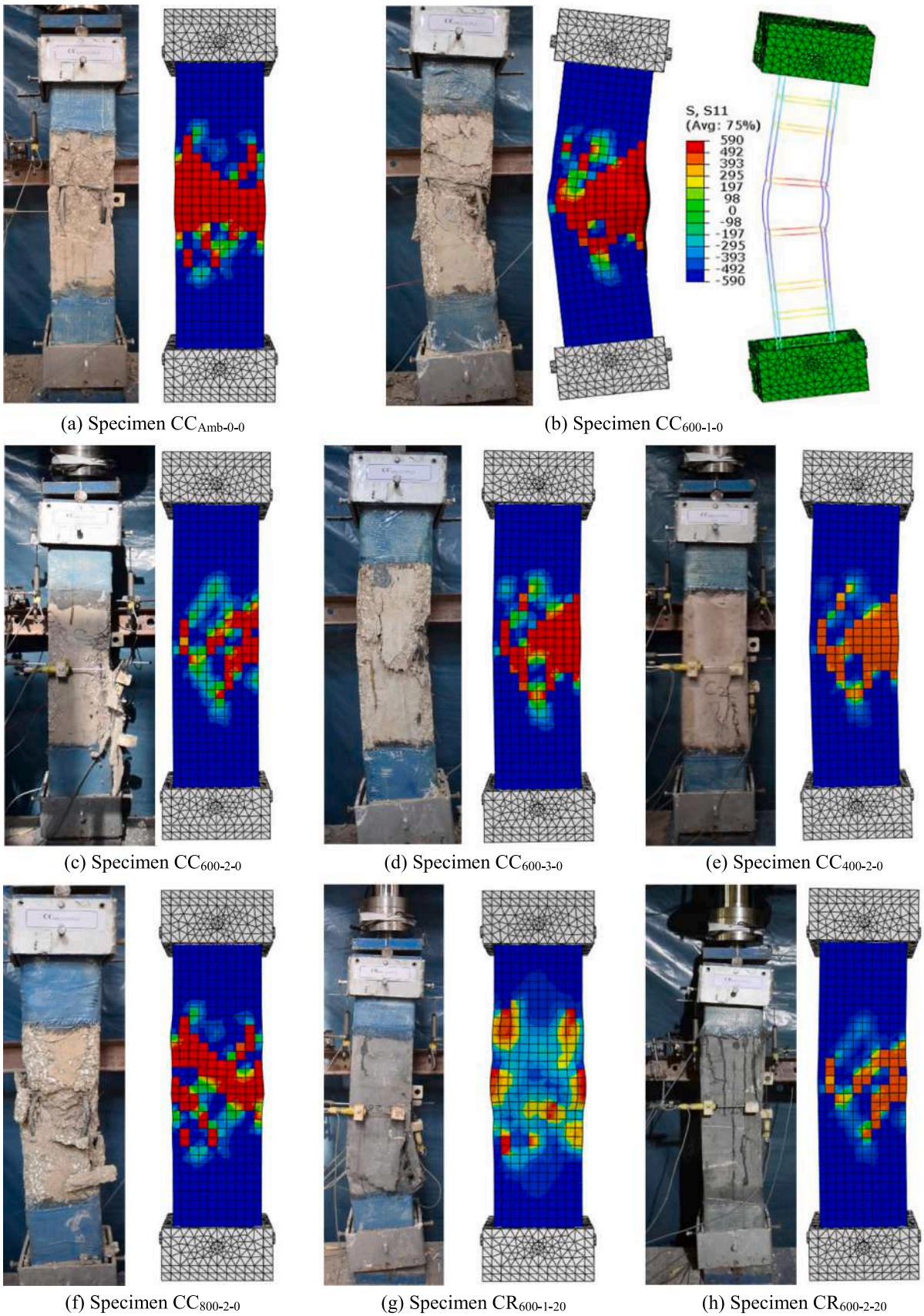
5.5. FEM results and validations

Table 8 presents the experimental and numerical outcomes in the ultimate loading stage for both the ultimate capacity and its corresponding displacement. The mean, standard deviation, and coefficient of variation were calculated for the results, which showed a good agreement between the experimental and numerical outcomes. Additionally, all numerical failure patterns of the tested columns are compared to the experimental ones as presented in Fig. 20, and a significant level of agreement is evident. The load-displacement relationships were presented in Fig. 21 in order to check the validity of the

Table 8
Experimental and numerical validations for the ultimate loading stage.

Group No.	Specimen ID	Ultimate axial load			Ultimate axial displacement		
		$P_{u,Exp.}$ (kN)	$P_{u,FE}$ (kN)	$P_{u,FE}/P_{u,Exp.}$	$\Delta_{u,Exp.}$ (mm)	$\Delta_{u,FE}$ (mm)	$\Delta_{u,FE}/\Delta_{u,Exp.}$
Control	$CC_{Amb-0-0}$	928	960	1.03	3.90	3.99	1.02
Group I	$CC_{600-1-0}$	673	702	1.04	4.24	4.35	1.02
	$CC_{600-2-0}$	473	495	1.05	5.19	5.29	1.02
	$CC_{600-3-0}$	335	358	1.07	5.75	5.86	1.02
Group II	$CC_{400-2-0}$	711	735	1.03	4.30	4.37	1.02
	$CC_{800-2-0}$	339	373	1.10	7.69	8.01	1.04
Group III	$CR_{600-1-20}$	1378	1413	1.03	4.85	4.96	1.02
	$CR_{600-2-20}$	1284	1311	1.02	4.77	4.98	1.04
	$CR_{600-3-20}$	1082	1113	1.03	4.52	4.69	1.04
Group IV	$CR_{400-2-20}$	1400	1444	1.03	5.00	5.32	1.06
	$CR_{800-2-20}$	1181	1215	1.03	4.73	4.95	1.05
Group V	$CR_{600-2-30}$	1807	1862	1.03	6.58	6.99	1.06
	$CR_{600-2-40}$	2326	2388	1.03	7.03	7.55	1.07
Average				1.04			1.04
Standard deviation (STDEV.)				0.022			0.018
Coefficient of variation (COV.) %				2.10 %			1.70 %

$P_{u,Exp.}$ = the experimental load-carrying capacity, $P_{u,FE}$ = the numerical load-carrying capacity; $\Delta_{u,Exp.}$ = the experimental ultimate axial displacement, $P_{u,FE}$ = the numerical ultimate axial displacement.

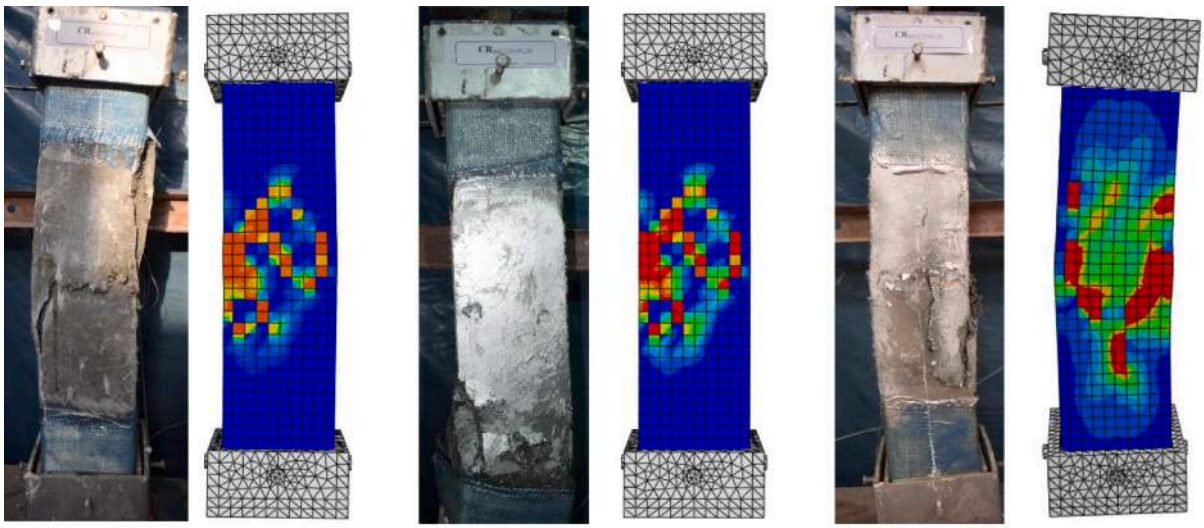


(a) Specimen $CC_{Amb-0-0}$ (b) Specimen $CC_{600-1-0}$

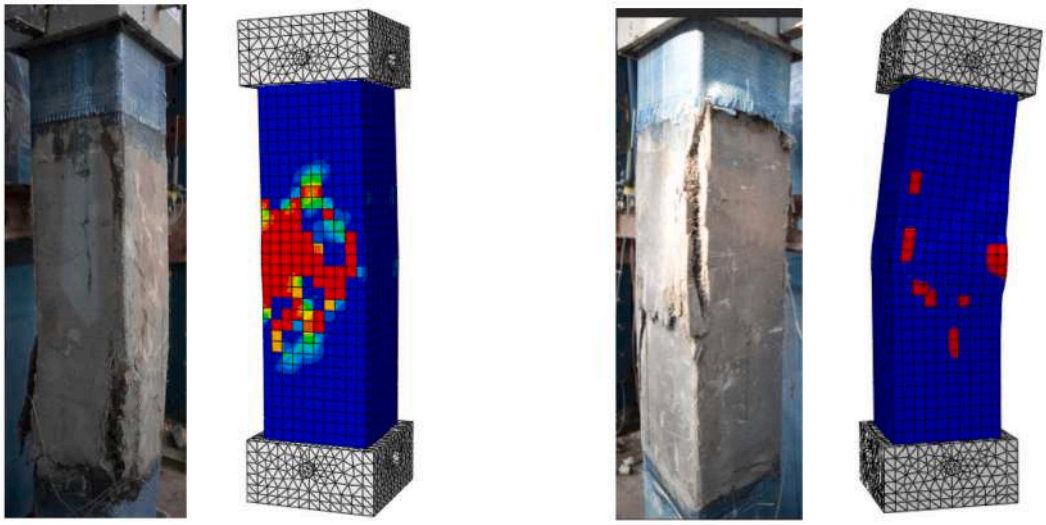
(c) Specimen $CC_{600-2-0}$ (d) Specimen $CC_{600-3-0}$ (e) Specimen $CC_{400-2-0}$

(f) Specimen $CC_{800-2-0}$ (g) Specimen $CR_{600-1-20}$ (h) Specimen $CR_{600-2-20}$

Fig. 20. Experimental versus numerical craking patterns at failure.,.



(i) Specimen $CR_{600\text{-}3\text{-}20}$ (j) Specimen $CR_{400\text{-}2\text{-}20}$ (k) Specimen $CR_{800\text{-}2\text{-}20}$



(l) Specimen $CR_{600\text{-}2\text{-}30}$ (m) Specimen $CR_{600\text{-}2\text{-}40}$

Fig. 20. (*continued*).

presented numerical model. In sum, the results showed that the used models were effective in capturing the overall experimental performance of the tested columns.

6. Theoretical analysis

6.1. A proposed equation for calculating the axial capacities (P_u)

The ultimate axial capacities (P_u) for non-repaired RC columns (both non-damaged and post-fire) can be estimated according to the formula adopted by ACI 318–19 [62] as follows:

$$P_u = \alpha_c f'_c (A_c - A_{st}) + A_{st} f_y \tag{14}$$

where α_c is a strength reduction factor that is taken to equal 0.85; f'_c is the specified cylinder compressive strength of concrete; A_c is the gross area of column section; A_{st} is the total area of longitudinal steel bars; and f_y is the yield strength of longitudinal steel.

On the other hand, for SHCC-repaired columns, the ultimate axial capacity (P_u) can be calculated by summation of the axial capacities of confined concrete core (P_{core}), longitudinal steel reinforcement (P_{st}), SHCC jacket (P_{SHCC}), and steel embedded inside SHCC jacket ($P_{st,J}$), as given in Eq. (15).

$$\begin{aligned} P_n &= P_{core} + P_{st} + P_{SHCC} + P_{st,J} \\ &= \alpha_c f'_{cc}(A_c - A_{st}) + A_{st} f_y + \alpha_c f'_{SHCC}(A_{SHCC} - A_{st,J}) + A_{st,J} f_{y,J} \end{aligned} \tag{15}$$

where f'_{SHCC} is the cylinder compressive strength of the SHCC; A_{SHCC} is the cross-sectional area of the SHCC jacket; $A_{st,J}$ is the area of the longitudinal reinforcement embedded inside the SHCC jacket; $f_{y,J}$ is the yield strength of the SHCC-embedded reinforcement; and f'_{cc} is the confined concrete strength of the post-fire core, determined by the model proposed by Xie et al. [80] as follows:

$$\frac{f'_{cc}}{f'_{co}} = 1 + 3.5\frac{f_{l,total}}{f'_{co}} \tag{16}$$

where f'_{co} is the cylinder compressive strength of unconfined concrete core and $f_{l,total}$ is the hoop confining pressure of concrete core, which is provided by both SHCC jacket $\left(f_{l,SHCC}\right)$ and stirrups $(f_{l,stirrup})$, as shown in Fig. 22.

Since the confining effect concentrates at the corner regions in square columns, an equivalent circular section with an effective diameter ($D_e = \sqrt{2} \times B$) was employed by Lam and Teng [90] to replace the square section (see Fig. 23), where B is the side length of the square

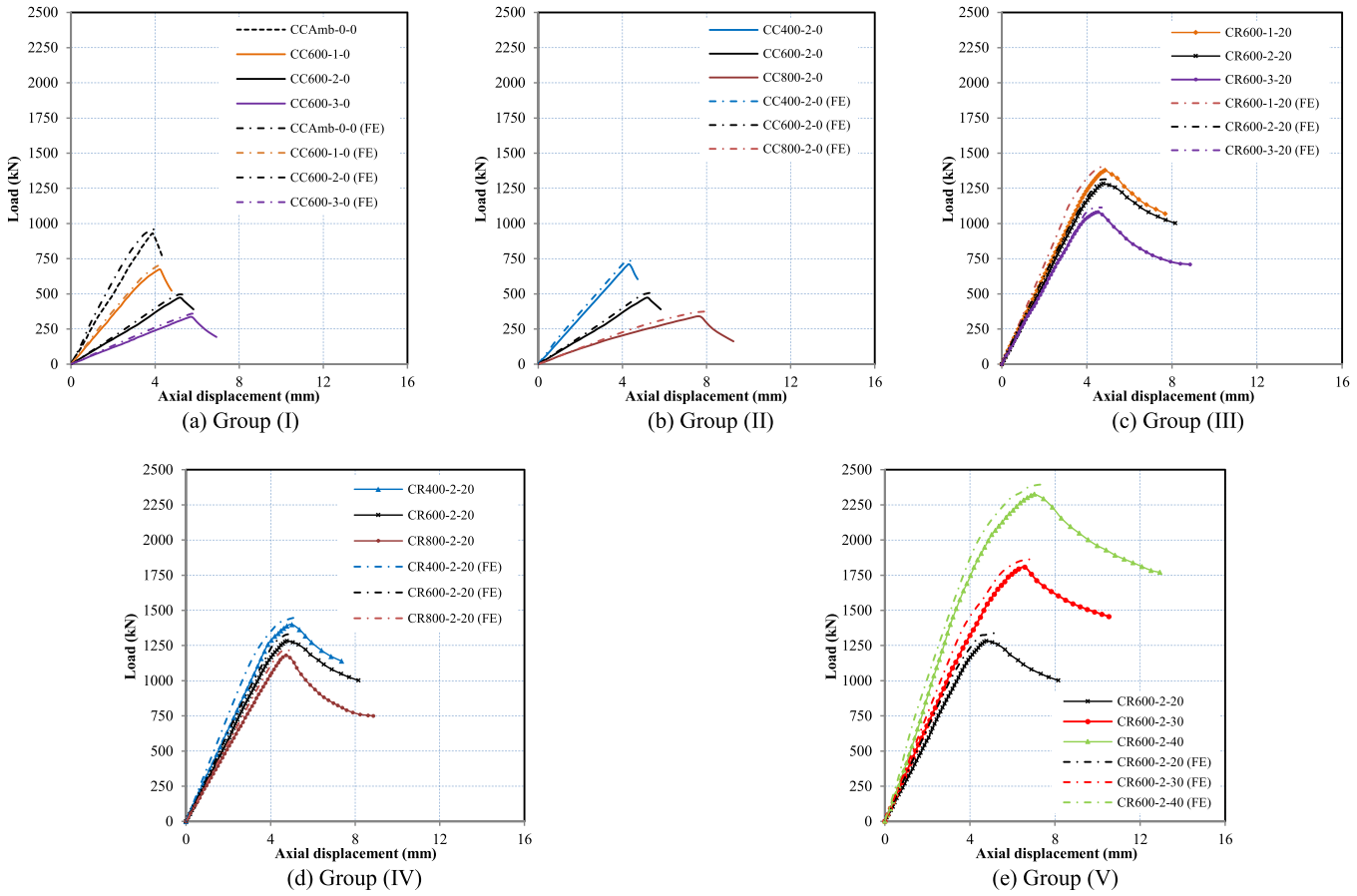


Fig. 21. Experimental versus numerical load-axial displacement responses.

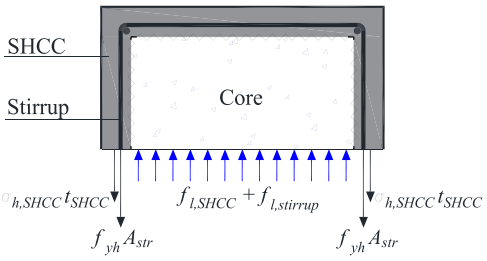


Fig. 22. Diagram of a square cross-section confined with a SHCC jacket.

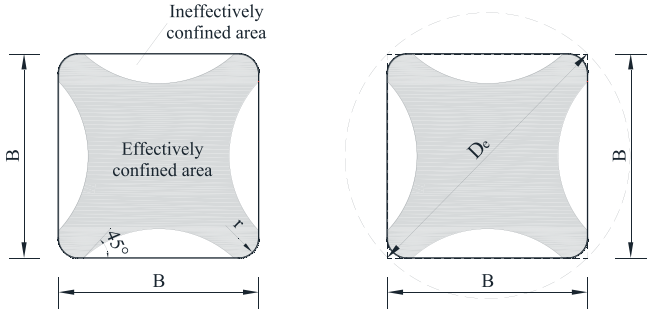


Fig. 23. Equivalent circular cross section [90].

cross-section. Then, based on the free-body diagram adopted in Fig. 22, the value of $f_{l,SHCC}$ can be determined as follows:

$$f_{l,SHCC} = k \times \frac{2 \times t_{SHCC} \times \sigma_{h,SHCC}}{D_e + t_{SHCC}} \tag{17}$$

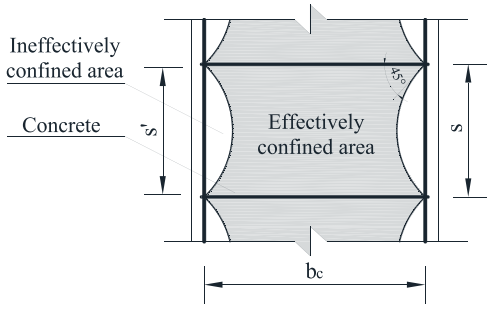


Fig. 24. Confining effect of stirrups [92].

where t_{SHCC} is the thickness of the SHCC jacket; $\sigma_{h,SHCC}$ is the effective stress level in the SHCC at failure and can be considered as the tensile strength of SHCC, which is determined by the uniaxial tensile test (see Fig. 2); and k is the horizontal confinement effectiveness coefficient taking into account the presence of ineffectively confined area of the concrete core (see Fig. 23), which can be determined by Eq. (18) as recommended by ACI 440.3R-04 [91].

$$k = \frac{A_e}{A_c} = \frac{1 - \left[\frac{2(B-2r)^2}{3B^2}\right] - \rho_g}{1 - \rho_g} \tag{18}$$

where A_e is the cross-sectional area of effectively confined concrete core; r is the fillet radius; and ρ_g is the core longitudinal reinforcement ratio.

As per stirrups (see Fig. 24), according to Mander et al. [92], the

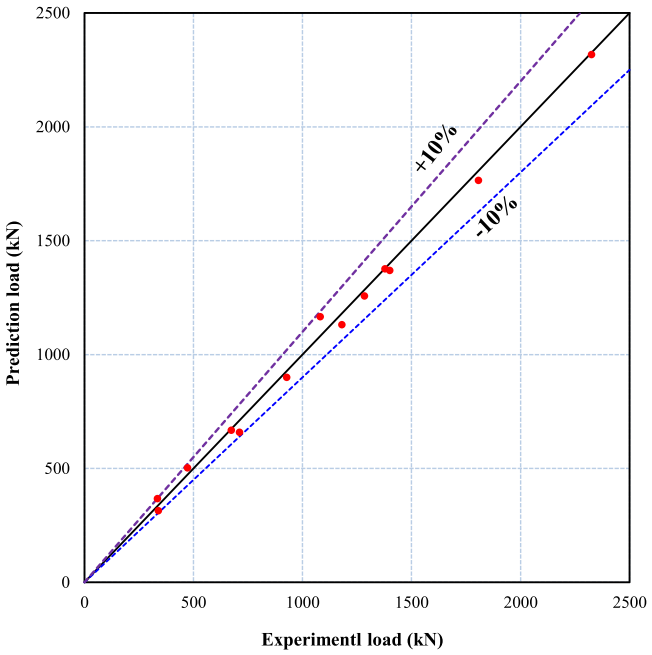


Fig. 25. Prediction capacities versus experimental results.

effective confining pressure ($f_{l,stirrup}$) can be expressed in Eq. (19).

$$f_{l,stirrup} = \frac{1}{2} k_e f_l \tag{19}$$

Where f_l is the lateral confining pressure on concrete core and can be calculated based on the equilibrium condition described in Eq. (20).

$$f_l \times s \times b_c = 2 \quad f_{yh} \times A_{str} \tag{20}$$

Where s is the spacing between center lines of stirrups; b_c is the width of stirrup between bar centers; f_{yh} is the yield strength of the stirrup; and A_{str} is the area of the stirrup bar.

Due to the arching effect that takes place between the discrete stirrups, as shown in Fig. 24, confinement nonuniformity from stirrups should be considered through the effectiveness coefficient k_e, which can be calculated in accordance with Mander et al. [92].

$$k_e = \frac{\left(1 - \sum_{i=1}^{n} \frac{(w'_i)^2}{6b_c^2}\right)\left(1 - \frac{s'}{2b_c}\right)^2}{1 - \rho_{cc}} \tag{21}$$

Where w'_i is the clear spacing of longitudinal bars; s' is the clear vertical spacing between stirrup bars; and ρ_{cc} is the ratio of longitudinal reinforcement area to the core cross-sectional area.

6.2. Verification of the proposed axial capacity equation against the experimental results

For verification purposes, the experimental results for the tested columns considering all studied parameters were compared with those obtained from the proposed equation, as illustrated in Fig. 25. It can be noticed that acceptable axial capacities are obtained by the proposed equation. Moreover, the variation in results ranged between 0 % and 9 % and the coefficient of variation (COV) was approximately 5 %.

7. Conclusion

This paper provides an insight into the repair of post-fire square RC columns with strain-hardening cementitious composites (SHCC) when subjected to axial compression. It should be explicitly stated that the tested columns were on a one-third scale. Based on the studied parameters, along with the results and discussions presented in this study, the following conclusions can be drawn:

1. The load-carrying capacity of the post-fire columns was significantly reduced due to the fire. This reduction varied between 23 % and 64 %, depending on the fire duration or temperature level.
2. Regardless of the studied parameters, using the SHCC jacket has substantially restored the axial capacity of all post-fire specimens. The increase in the ultimate load (P_u) as compared to the reference non-damaged specimen ($CC_{Amb\text{-}0\text{-}0}$) varied between 17 % and 151 %.
3. Utilization of SHCC jackets enhanced the failure mode due to the superior characteristics of the SHCC. Furthermore, there was no evidence of delamination or debonding between the SHCC and the post-fire concrete core.
4. Fire exposure led the concrete to become more permeable, resulting in a considerable decrease in the stiffness of the post-fire columns. However, the repairing system (SHCC jacket) improved the deformational characteristics and the axial stiffness of the repaired specimens.
5. Applying three SHCC jacket thicknesses of 20, 30, and 40 mm considerably improves the ultimate load-carrying capacity and the axial stiffness at almost a similar rate as the increase in the jacketing area due to the extra contribution of SHCC material.
6. The repaired columns exhibited an outstanding improvement in energy absorption, with a 238 % average increase relative to the reference non-damaged specimen ($CC_{Amb\text{-}0\text{-}0}$).
7. It is shown that the proposed FEM model adopted for numerical analysis of the SHCC-repaired specimens is capable of predicting the ultimate capacity, failure mode, and the overall experimental performance of the tested columns reasonably accurately, allowing future work to extend the analysis beyond existing test cases.
8. A simple proposed equation was presented for calculating the ultimate capacities of the tested SHCC-repaired columns with an acceptable coefficient of variation (COV) of 5 %, as demonstrated by the comparisons between the experimental data and the estimated values.

8. Recommendations for future work

While this work does provide some important conclusions, further study is required to fully understand the performance of fire-damaged columns repaired by SHCC jacket. The following are some of the key recommendations for further research in this area:

1. The square RC columns tested in this investigation are one-third scale. However, to thoroughly investigate the efficiency of the SHCC jackets, full-scale RC columns of varying cross-sectional shapes are necessary.
2. An experimental program on post-fire RC columns repaired using SHCC and subjected to cyclic loads should be conducted.
3. It is important to study how the slenderness ratio affects the behavior of post-fire and post-fire/repaired RC columns.

Funding

The author(s) received no financial support for the research, authorship, and/or publication of this article.

CRediT authorship contribution statement

Abd El-Hakim A. Khalil: Supervision, Conceptualization. **Ahmed T. Baraghith:** Writing – review & editing, Writing – original draft, Resources, Methodology, Investigation, Formal analysis, Data curation, Conceptualization. **Tarek F. Elshafiey:** Supervision, Conceptualization. **Hanan Ali:** Resources, Data curation. **Reda N. Behiry:** Writing – review

& editing, Writing – original draft, Resources, Methodology, Investigation, Formal analysis, Data curation, Conceptualization.

Declaration of Competing Interest

The author(s) declared no potential conflicts of interest with respect to the research, authorship, and/or publication of this article.

Data availability

No data was used for the research described in the article.

References

[1] Ashteyat AM, Hanandeh S, Al-Btoush AY. Behavior of heat damaged circular reinforced concrete columns repaired using Carbon Fiber Reinforced Polymer rope. J Build Eng 2020;31:101424. https://doi.org/10.1016/j.jobe.2020.101424..

[2] Al-Nimry H, Haddad R, Afram S, Abdel-Halim M. Effectiveness of advanced composites in repairing heat-damaged RC columns. Mater Struct 2013;46(11): 1843–60. https://doi.org/10.1617/s11527-013-0022-8..

[3] Xu J. Circular reinforced concrete columns damaged by fire and retrofitted with CFRP and steel jacketing (Doctoral dissertation). New York, USA: Syracuse University; 2022.

[4] ISO 834. Fire resistance tests - Elements of building construction. Geneva, Switzerland: International Organization for Standardization; 2014.

[5] ASTM E119-20. Standard test methods for fire tests of building construction and materials. West Conshohocken, PA: ASTM International; 2020.

[6] Moghtadernejad N, Jamshidi M, Maheri MR, Keong CK. Repair of post-heated short rectangular reinforced concrete columns with FRP jackets. In Structures, 34. Elsevier,; 2021. p. 4269–83. https://doi.org/10.1016/j.istruc.2021.10.038..

[7] Liu WW, Ouyang LJ, Gao WY, Liang J, Wang TC, Song J, et al. Repair of fire-damaged RC square columns with CFRP textile-reinforced ECC matrix. Eng Struct 2023;292:116530. https://doi.org/10.1016/j.engstruct.2023.116530..

[8] Buchanan AH, Abu AK. Structural design for fire safety. 2nd ed..,. Chichester, UK: John Wiley & Sons Ltd.; 2017. p. 2017.

[9] Naus D. A compilation of elevated temperature concrete material property data and information for use in assessments of nuclear power plant reinforced concrete structures. Washington, DC: US Nuclear Regulatory Commission, Office of Nuclear Regulatory Research; 2010.

[10] Mehboob S. Effect of FRP on compressive strength of unheated and post heated concrete. Life Sci J 2013;10(12s).

[11] Raut NK, Kodur VKR. Response of high-strength concrete columns under design fire exposure. J Struct Eng 2011;137(1):69–79. https://doi.org/10.1061/(asce)st.1943-541x.0000265..

[12] Li X, Lu X, Qi J, Bao Y. Flexural behavior of fire-damaged concrete beams repaired with strain-hardening cementitious composite. Eng Struct 2022;261:114305. https://doi.org/10.1016/j.engstruct.2022.114305..

[13] Zhang P, Kang L, Wang J, Guo J, Hu S, Ling Y. Mechanical properties and explosive spalling behavior of steel-fiber-reinforced concrete exposed to high temperature-a review. Appl Sci 2020;10(7):2324. https://doi.org/10.3390/app10072324.

[14] Yermak N, Pliya P, Beaucour AL, Simon A, Noumowé A. Influence of steel and/or polypropylene fibres on the behaviour of concrete at high temperature: Spalling, transfer and mechanical properties. Constr Build Mater 2017;132:240–50. https://doi.org/10.1016/j.conbuildmat.2016.11.120.

[15] Ma Q, Guo R, Zhao Z, Lin Z, He K. Mechanical properties of concrete at high temperature-A review. Constr Build Mater 2015;93:371–83. https://doi.org/10.1016/j.conbuildmat.2015.05.131.

[16] Debicki G, Haniche R, Delhomme F. An experimental method for assessing the spalling sensitivity of concrete mixture submitted to high temperature. Cem Concr Compos 2012;34(8):958–63. https://doi.org/10.1016/j.cemconcomp.2012.04.002.

[17] Wang Z, Zhong Y, Jiang K, Su M, Zhao O. Post-fire behaviour and resistances of square recycled aggregate concrete-filled stainless steel tube stub columns. Thin-Walled Struct, p 2024:111564. https://doi.org/10.1016/j.tws.2024.111564.

[18] Lie TT, Woollerton JL. . Fire resistance of reinforced concrete columns: test results. National Research Council Canada, Institute for Research in Construction; 1988. https://doi.org/10.1520/stp35297s.

[19] Dotreppe JC, Franssen JM, Bruls A, Baus R, Vandevelde P, Minne R, et al. Experimental research on the determination of the main parameters affecting the behaviour of reinforced concrete columns under fire conditions. Mag Concr Res 1997;49(179):117–27. https://doi.org/10.1680/macr.1997.49.179.117.

[20] Chan YN, Peng GF, Anson M. Residual strength and pore structure of high-strength concrete and normal strength concrete after exposure to high temperatures. Cem Concr Compos 1999;21(1):23–7. https://doi.org/10.1016/s0958-9465(98)00034-1.

[21] Aldea CM, Franssen JM, Dotreppe JC. Fire test on normal and high-strength reinforced concrete columns. Int Workshop Fire Perform High-Strength Concr 1997.

[22] Kodur V, Mcgrath R. Fire endurance of high strength concrete columns. Fire Technol 2003;39(1):73–87. https://doi.org/10.1023/A:1021731327822.

[23] Chen YH, Chang YF, Yao GC, Sheu MS. Experimental research on post-fire behaviour of reinforced concrete columns. Fire Saf J 2009;44(5):741–8. https://doi.org/10.1016/j.firesaf.2009.02.004.

[24] Wu B, Hong Z, Tang GH, Wang C. Fire resistance of reinforced concrete columns with square cross section. Adv Struct Eng 2007;10(4):353–69. https://doi.org/10.1260/136943307783239336.

[25] Kodur VKR, Raut NK, Mao XY, Khaliq W. Simplified approach for evaluating residual strength of fire-exposed reinforced concrete columns. Mater Struct 2013; 46(12):2059–75. https://doi.org/10.1617/s11527-013-0036-2.

[26] Hibner DR. Residual axial capacity of fire exposed reinforced concrete columns. Michigan, USA: Michigan State University; 2017. https://doi.org/10.1016/j.proeng.2017.11.116.

[27] Buch SH, Sharma UK. Fire resistance of eccentrically loaded reinforced concrete columns. Fire Technol 2019;55(5):1517–52. https://doi.org/10.1007/s10694-019-00823-x.

[28] Sharma A, Bošnjak J, Bessert S. Experimental investigations on residual bond performance in concrete subjected to elevated temperature. Eng Struct 2019;187: 384–95. https://doi.org/10.1016/j.engstruct.2019.02.061.

[29] Nair A, Salem OS. Experimental determination of the residual compressive strength of concrete columns subjected to different fire durations and load ratios. J Struct Fire Eng 2020. https://doi.org/10.1108/jsfe-10-2019-0034.

[30] Al-Naqeeb F, Al-Thairy H. The behavior of reinforced concrete columns exposure to eccentric loads at high temperature. Journal of Physics: Conference Series, 1895. IOP Publishing,; 2021, 012055. https://doi.org/10.1088/1742-6596/1895/1/012055.

[31] Yaqub M, Bailey CG, Nedwell P. Axial capacity of post-heated square columns wrapped with FRP composites. Cem Concr Compos 2011;33(6):694–701. https://doi.org/10.1016/j.cemconcomp.2011.03.011..

[32] Yaqub M, Bailey CG, Nedwell P, Khan QUZ, Javed I. Strength and stiffness of post-heated columns repaired with ferrocement and fibre reinforced polymer jackets. Compos B Eng 2013;44(1):200–11. https://doi.org/10.1016/j.compositesb.2012.05.041..

[33] Abadel AA, Khan MI, Masmoudi R. Axial capacity and stiffness of post-heated circular and square columns strengthened with carbon fiber reinforced polymer jackets. Structures, 33. Elsevier,; 2021. p. 2599–610. https://doi.org/10.1016/j.istruc.2021.05.081..

[34] Al-Kamaki YS, Al-Mahaidi R, Bennetts I. Experimental and numerical study of the behaviour of heat-damaged RC circular columns confined with CFRP fabric. Compos Struct 2015;133:679–90. https://doi.org/10.1016/j.compstruct.2015.07.116.

[35] Zhou J, Wang L. Repair of fire-damaged reinforced concrete members with axial load: a review. Sustainability 2019;11(4):963. https://doi.org/10.3390/su11040963.

[36] Zahid MM, Bakar BA, Nazri FM, Ahmad MM, Muhamad K. Review of repair materials for fire-damaged reinforced concrete structures. IOP Conference Series: Materials Science and Engineering, 318. IOP Publishing; 2018, 012023. https://doi.org/10.1088/1757-899x/318/1/012023.

[37] Chinthapalli HK, Chellapandian M, Agarwal A, Prakash SS. Effectiveness of hybrid fibre-reinforced polymer retrofitting on behaviour of fire damaged RC columns under axial compression. Eng Struct 2020;211:110458. https://doi.org/10.1016/j.engstruct.2020.110458.

[38] Al-Nimry HS, Ghanem AM. FRP confinement of heat-damaged circular RC columns. Int J Concr Struct Mater 2017;11(1):115–33. https://doi.org/10.1007/s40069-016-0181-4.

[39] Usman M, Yaqub M, Auzair M, Khaliq W, Noman M, Afaq A. Restorability of strength and stiffness of fire damaged concrete using various composite confinement techniques. Constr Build Mater 2021;272:121984. https://doi.org/10.1016/j.conbuildmat.2020.121984..

[40] Li V.C., 1992. Performance driven design of fiber reinforced cementitious composites. In: R.N. Swamy (Ed.) 4th RILEM International Symposium on Fiber Reinforced Concrete, 12–30. https://doi.org/10.1201/9781482271225–8.

[41] Li VC. Engineered cementitious composites (ECC) material, structural, and durability performance. In: Nawy EG, editor. Concrete Construction Engineering Handbook. CRC Press; 2008.

[42] Li, V. and Fischer, G., 2006. International RILEM Workshop on High Performance Fiber Reinforced Cementitious Composites (HPFRCC) in Structural Applications: Proceedings. RILEM.

[43] Li WW, Liu J, Lin QX, Yang X, Shumuye ED, Peng W. Behavior of FRP-engineered cementitious composite layer and concrete interface with FRP anchors. Eng Struct 2024;303:117526. https://doi.org/10.1016/j.engstruct.2024.117526.

[44] Ding M, Xu W, Wang J, Chen Y, Fang R, Zhou D, et al. Seismic performance and estimation of flexural bearing capacity of prefabricated engineered cementitious composite shell-reinforced concrete composite column with grouted sleeve connection. Soil Dyn Earthq Eng 2024;178:108430. https://doi.org/10.1016/j.soildyn.2023.108430.

[45] Afefy HM, Baraghith AT, Hassan A, Abuzaid MK. Strengthening of shear-deficient RC beams using near surface embedded precast cement-based composite plates (PCBCPs). Eng Struct 2021;244:112765. https://doi.org/10.1016/j.engstruct.2021.112765.

[46] Baraghith AT, Mansour W, Behiry RN, Fayed S. Effectiveness of SHCC strips reinforced with glass fiber textile mesh layers for shear strengthening of RC beams: Experimental and numerical assessments. Constr Build Mater 2022;327:127036. https://doi.org/10.1016/j.conbuildmat.2022.127036.

[47] Baraghith AT, Khalil AHA, Etman EE, Behiry RN. Improving the shear behavior of RC dapped-end beams using precast strain-hardening cementitious composite (P-

SHCC) plates. Structures, 50. Elsevier; 2023. p. 978–97. https://doi.org/10.1016/j.istruc.2023.02.059.
[48] Elnagar AB, Afefy HM, Baraghith AT, Mahmoud MH. Experimental and numerical investigations on the impact resistance of SHCC-strengthened RC slabs subjected to drop weight loading. Constr Build Mater 2019;229:116866. https://doi.org/10.1016/j.conbuildmat.2019.116866.
[49] Khalil AA, El Shafiey TF, Mahmoud MH, Baraghith AT, Etman AE. Shear behavior of innovated composite hollow core slabs. Int Conf Adv Struct Geotech Eng 2019.
[50] Afefy HM, Baraghith AT, Mahmoud MH. Retrofitting of defected reinforced-concrete cantilever slabs using different techniques. Mag Concr Res 2020;72(14):703–19. https://doi.org/10.1680/jmacr.18.00340.
[51] Khalil AEH, Etman E, Atta A, Essam M. Behavior of RC beams strengthened with strain hardening cementitious composites (SHCC) subjected to monotonic and repeated loads. Eng Struct 2017;140:151–63. https://doi.org/10.1016/j.engstruct.2017.02.049.
[52] Li K, Wei Y, Li Y, Li Z, Zhu J. Flexural behavior of reinforced concrete beams strengthened with high-strength stainless steel wire rope meshes reinforced ECC. Constr Build Mater 2023;362:129627. https://doi.org/10.2139/ssrn.4196443.
[53] Zhou C, Xie Y, Wang W, Zheng Y. Performance-based design for improving impact resistance of RC bridge piers with CFRP grid-reinforced ECC. Eng Struct 2023;275:115217. https://doi.org/10.1016/j.engstruct.2022.115217.
[54] Li X, Bao Y, Xue N, Chen G. Bond strength of steel bars embedded in high-performance fiber-reinforced cementitious composite before and after exposure to elevated temperatures. Fire Saf J 2017;92:98–106. https://doi.org/10.1016/j.firesaf.2017.06.006.
[55] Zhang Z, Liu JC, Xu X, Yuan L. Effect of sub-elevated temperature on mechanical properties of ECC with different fly ash contents. Constr Build Mater 2020;262:120096. https://doi.org/10.1016/j.conbuildmat.2020.120096.
[56] Li X, Xu H, Meng W, Bao Y. Tri-axial compressive properties of high-performance fiber-reinforced cementitious composites after exposure to high temperatures. Constr Build Mater 2018;190:939–47. https://doi.org/10.1016/j.conbuildmat.2018.09.150.
[57] ASTM C39/C39M-21. Standard test method for compressive strength of cylindrical concrete specimens. ASTM International; 2021. ⟨www.astm.org⟩.
[58] ASTM C469/C469M-14. Standard test method for static modulus of elasticity and Poisson's ratio of concrete in compression. ASTM International,; 2014. ⟨www.astm.org⟩.
[59] ASTM D2936-20. Standard test method for direct tensile strength of intact rock core specimens. ASTM International; 2020. ⟨www.astm.org⟩.
[60] Khalil AHA, Atta AM, Baraghith AT, Behiry RN, Soliman OE. Shear strengthening of concrete deep beams using pre-fabricated strain-hardening cementitious composite plates. Eng Struct 2023;278:115548. https://doi.org/10.1016/j.engstruct.2022.115548..
[61] ASTM A615/A615M-16. Standard specification for deformed and plain carbon steel bars for concrete reinforcement. ASTM International; 2016. ⟨www.astm.org⟩.
[62] ACI Committee. Building code requirements for structural concrete (ACI 318-19) and commentary. Farmington Hills, MI: American Concrete Institute; 2019. p. 519.
[63] EN 1992-1-2. Eurocode 2: Design of concrete structures-Part 1-2: general rules structural fire design.. Brussels: European Committee for Standardization; 2004. p. 2004.
[64] Zhao J, Wang K, Wang S, Wang Z, Yang Z, Shumuye ED, et al. Effect of elevated temperature on mechanical properties of high-volume fly ash-based geopolymer concrete, mortar and paste cured at room temperature. Polymers 2021;13(9):1473. https://doi.org/10.3390/polym13091473.
[65] Shumuye ED, Zhao J, Wang Z. Effect of the curing condition and high-temperature exposure on ground-granulated blast-furnace slag cement concrete. IJCSM 2021;15:1–20. https://doi.org/10.1186/s40069-020-00437-6.
[66] Ashteyat AM, Obaidat YT, Al-Btoush AY, Hanandeh S. Experimental and numerical study of strengthening and repairing heat-damaged RC circular column using hybrid system of CFRP. Case Stud Constr Mater 2021;15:e00742. https://doi.org/10.1016/j.cscm.2021.e00742.
[67] Krishna A, Kaliyaperumal SRM. Effect of elevated temperature on strength and ductility of axially loaded hybrid fiber reinforced concrete columns (December). Structures, 34. Elsevier; 2021. p. 3548–56. https://doi.org/10.1016/j.istruc.2021.09.099 (December).
[68] Jafarzadeh H, Nematzadeh M. Flexural strengthening of fire-damaged GFRP-reinforced concrete beams using CFRP sheet: Experimental and analytical study. Compos Struct 2022;288:115378. https://doi.org/10.1016/j.compstruct.2022.115378.
[69] Hager I. Colour change in heated concrete. Fire Technol 2014;50:945–58. https://doi.org/10.1007/s10694-012-0320-7.
[70] ACI Committee 228.2R-13. Report on Nondestructive Test Methods for Evaluation of Concrete in Structures. Farmington Hills, Michigan: American Concrete Institute; 2013.
[71] Hager I, Krakowska P, Technologii K, Budowlanych M, Budowli O. Methods for assessing the state of concrete in fire damaged structures. Cem Wapno Beton 2009;4:167–78.
[72] Dilek U, Leming ML. Comparison of pulse velocity and impact-echo findings to properties of thin disks from a fire damaged slab. J Perform Constr Facil 2007;21(1):13–21. https://doi.org/10.1061/(ASCE)0887-3828(2007)21:1(13).
[73] Colombo M, Felicetti R. New NDT techniques for the assessment of fire-damaged concrete structures. Fire Saf J 2007;42(6-7):461–72. https://doi.org/10.1016/j.firesaf.2006.09.002.
[74] Wróblewska J, Kowalski R. Assessing concrete strength in fire-damaged structures. Constr Build Mater 2020;254:119122. https://doi.org/10.1016/j.conbuildmat.2020.119122.
[75] Ingham J, Tarada F. Turning up the heat-full service fire safety engineering for concrete structures. Concr-Lond-Concr Soc 2007;41(9):27.
[76] ASTM C881/C881M-20, 2020. Standard Specification for Epoxy-Resin-Base Bonding Systems for Concrete. West Conshohocken, PA: ASTM International; 2020.
[77] Abo-Zaid L, Hassan A, Abdel-Hafez LM. Repairing post-heated L-shaped RC columns with advanced thin concrete jacketing. Constr Build Mater 2019;221:573–85. https://doi.org/10.1016/j.conbuildmat.2019.06.101.
[78] Lai BL, Zhang MY, Chen ZP, Liew JR, Zheng YY. Axial compressive behavior and design of semi-precast steel reinforced concrete composite columns with permanent ECC formwork (November). Structures, 57. Elsevier; 2023, 105130. https://doi.org/10.1016/j.istruc.2023.105130 (November).
[79] Hossain KMA, Parajuli S, Manzur T. Axial behavior of columns confined with engineered cementitious composite. Acids Struct J 2022;119(1):67–76. https://doi.org/10.14359/51734217.
[80] Xie J, Fu Q, Yan JB. Compressive behaviour of stub concrete column strengthened with ultra-high performance concrete jacket. Constr Build Mater 2019;204:643–58. https://doi.org/10.1016/j.conbuildmat.2019.01.220..
[81] Chen X, Zhuge Y, Al-Gemeel AN, Xiong Z. Compressive behaviour of concrete column confined with basalt textile reinforced ECC. Eng Struct 2021;243:112651. https://doi.org/10.1016/j.engstruct.2021.112651.
[82] Hassan A, Baraghith AT, Atta AM, El-Shafiey TF. Retrofitting of shear-damaged RC T-beams using U-shaped SHCC jacket. Eng Struct 2021;245:112892. https://doi.org/10.1016/j.engstruct.2021.112892..
[83] Song J, Gao WY, Ouyang LJ, Zeng JJ, Yang J, Liu WD. Compressive behavior of heat-damaged square concrete prisms confined with basalt fiber-reinforced polymer jackets. Eng Struct 2021;242:112504. https://doi.org/10.1016/j.engstruct.2021.112504..
[84] Hibbitt K. Sorensen: ABAQUS Theory manual, Version 6.1. Pawtucket: Hibbitt, Karlsson and Sorensen; 2000.
[85] EN 1993-1-2. Eurocode 3: design of steel structures-part 1–2: general rules-structural fire design. Brussels: European Committee for Standardization; 2005.
[86] EN 1991-1-2. Eurocode 1: actions on structures-part 1–2: general actions -actions on structures exposed to fire. Brussels: European Committee for Standardization; 2002.
[87] Ghalla M, Badawi M, Mlybari EA, Hu JW. Enhancing shear strength of RC beams through externally bonded reinforcement with stainless-steel strips and FRCM jacket to mitigate the failure risk. RINENG 2024;22:102246. https://doi.org/10.1016/j.rineng.2024.102246..
[88] Alharthai M, Bahrami A, Badawi M, Ghalla M, Elsamak G, Abdelmgeed FA. Numerical study on enhancing shear performance of RC beams with external aluminum alloy plates bonded using steel anchors. RINENG 2024;22:102143. https://doi.org/10.1016/j.rineng.2024.102143..
[89] Emara M, Elsamak G, Ghalla M, Hu JW, Badawi M, Salama MI. Shear improvement of defected RC beams with sustainable aluminum boxes incorporating high performance concretes. Case Stud Constr Mater 2024;21:e03500. https://doi.org/10.1016/j.cscm.2024.e03500.
[90] Lam L, Teng JG. Design-oriented stress-strain model for FRP-confined concrete in rectangular columns. J Reinf Plast Compos 2003;22(13):1149–86. https://doi.org/10.1177/0731684403035429.
[91] ACI 440.3R-04. Guide test methods for fiber-reinforced polymers for reinforcing or strengthening concrete structures. Michigan, USA: Farmington Hills; 2004.
[92] Mander JB, Priestley MJ, Park R. Theoretical stress-strain model for confined concrete. J Struct Eng 1988;114(8):1804–26. https://doi.org/10.1061/(asce)0733-9445(1988)114:8(1804).